İ. GÖKDEMİR

THERMOELASTIC ANALYSIS OF FUNCTIONALLY GRADED TUBES WITH TEMPERATURE DEPENDENT MATERIAL PROPERTIES

THE GRADUATE SCHOOL OF NATURAL AND APPLIED SCIENCES
OF
ATILIM UNIVERSITY

İREM GÖKDEMİR

A MASTER OF SCIENCE THESIS
IN
THE DEPARTMENT OF CIVIL ENGINEERING

SEPTEMBER 2024

ATILIM UNIVERSITY 2024

THERMOELASTIC ANALYSIS OF FUNCTIONALLY GRADED TUBES WITH TEMPERATURE DEPENDENT MATERIAL PROPERTIES

A THESIS SUBMITTED TO
THE GRADUATE SCHOOL OF NATURAL AND APPLIED SCIENCES
OF
ATILIM UNIVERSITY

BY

İREM GÖKDEMİR

IN PARTIAL FULFILLMENT OF THE REQUIREMENTS
FOR
THE DEGREE OF MASTER OF SCIENCE
IN
THE DEPARTMENT OF CIVIL ENGINEERING

SEPTEMBER 2024

Approval of the Graduate School of Natural and Applied Sciences, Atılım University.

Prof. Dr. Ender Keskinkılıç
Director

I certify that this thesis satisfies all the requirements as a thesis for the degree of **Master of Science in Civil Engineering, Atılım University.**

Prof. Dr. Yakup Darama
Head of Department

This is to certify that we have read the thesis THERMOELASTIC ANALYSIS OF FUNCTIONALLY GRADED TUBES WITH TEMPERATURE DEPENDENT MATERIAL PROPERTIES submitted by İREM GÖKDEMİR and that in our opinion it is fully adequate, in scope and quality, as a thesis for the degree of Master of Science.

Prof Dr. Hakan Argeşo
Co-Supervisor

Prof. Dr. Tolga Akış
Supervisor

Examining Committee Members

Asst. Prof. Dr. Hakan Kalkan
Manufacturing Eng. Department
Atılım University

Prof. Dr. Tolga Akış
Civil Eng. Department
Atılım University

Asst. Prof. Dr. Bahram Lotfi
Mechanical Eng. Department
TOBB University of Economics and Technology

Date: 09 September 2024

I hereby declare that all information in this document has been obtained and presented in accordance with academic rules and ethical conduct. I also declare that, as required by these rules and conduct, I have fully cited and referenced all material and results that are not original to this work.

Name, Last Name: İrem Gökdemir

Signature:

ABSTRACT

THERMOELASTIC ANALYSIS OF FUNCTIONALLY GRADED TUBES WITH TEMPERATURE DEPENDENT MATERIAL PROPERTIES

Gökdemir, İrem

M.S., Civil Engineering Department

Supervisor: Prof. Dr. Tolga Akış

Co-Supervisor: Prof. Dr. Ahmet Hakan Argeşo

September 2024, 83 pages

This study presents an investigation on the thermoelastic behavior of infinitely long functionally graded tubes with fixed ends that have temperature dependent material properties. The tubes are subjected to axisymmetric thermal and mechanical loadings. Polar coordinates are used in the derivations. The thermal problem is steady-state, and the formulation of mechanical problem is realized under the assumptions of small deformation theory and a state of plane strain. The thermal and mechanical properties of the tubes are assumed to be graded along the radial direction of the tube. The functionally graded material is assumed to be formed from two constituents, namely Inconel 718 and Ti-6Al-4V alloys. Rule of mixtures are used in the determination of effective material properties. The variations of the thermal and mechanical properties along the radial direction of the tube are described by a new form of gradation function. With this proposed function a smooth and controlled grading of the properties at the desired locations within the tube is possible. Sample problems are considered, and the solutions determined for the tubes made of homogeneous Inconel 718 and Ti-6Al-4V alloys are compared with those obtained for the tubes made of functionally graded materials. The results reveal that, with proper material gradation, the tubes made of functionally graded materials may become advantageous than those made of homogeneous materials that form the functionally graded tubes.

Keywords: Tube, Thermoelasticity, Functionally Graded Materials, Temperature Dependent Properties.

ÖZ

SICAKLIĞA BAĞLI MALZEME ÖZELLİKLERİNE SAHİP FONKSİYONEL DERECELENDİRİLMİŞ TÜPLERİN TERMOELASTİK ANALİZİ

Gökdemir, İrem
Yüksek Lisans, İnşaat Mühendisliği Bölümü
Danışman: Prof. Dr. Tolga Akış
Eş Danışman: Prof. Dr. Ahmet Hakan Argeşo
Eylül 2024, 83 sayfa

Bu çalışma sıcaklığa bağlı malzeme özelliklerine sahip fonksiyonel derecelendirilmiş, sonsuz uzunlukta ve uçları sabitlenmiş tüplerin termoelastik analizini içermektedir. Tüpler eksenel yönde simetrik termal ve mekanik yüklemeye maruz bırakılmıştır. Isı probleminde kararlı hal, mekanik problemde ise küçük şekil değiştirme teorisi ve düzlem gerilim durumu varsayımları göz önünde bulundurulmuştur. Tüplerin termal ve mekanik özellikleri tüpün radyal yönü boyunca değiştiği kabul edilmiştir. Fonksiyonel derecelendirilmiş malzemenin Inconel 718 ve Ti-6Al-4V alaşımları olmak üzere iki bileşenden oluştuğu varsayılmıştır. Malzemenin etkin özellikleri belirlenirken karışımlar kuralı kullanılmıştır. Bileşenlerin termal ve mekanik özelliklerinin tüpün radyal yönündeki değişimleri yeni bir derecelendirme fonksiyonu ile belirlenmiştir. Önerilen fonksiyon ile bileşenlerin özelliklerinin istenen lokasyonda düzgün ve kontrollü kademelendirilmesi mümkün olmuştur. Daha sonra örnek problemler çözülmüş ve bu problemlerde fonksiyonel derecelendirilmiş tüpler için elde edilen sonuçlar, Inconel 718 ve Ti-6Al-4V alaşımlarından yapılmış homojen tüplerin sonuçları ile karşılaştırılmıştır. Uygun malzeme derecelendirmesi yapıldığında, fonksiyonel derecelendirilmiş tüplerin, bu tüpleri oluşturan bileşenden yapılmış homojen tüplere göre avantajlı olduğu gösterilmiştir.

Anahtar Kelimeler: Tüp, Termoelastisite, Fonksiyonel Derecelendirilmiş Malzemeler, Sıcaklığa Bağlı Malzeme Özellikleri.

To My Beloved Family

ACKNOWLEDGMENTS

I would like to express my deepest gratitude and heartfelt appreciation to my thesis supervisors, Prof. Dr. Tolga Akış and Prof. Dr. Ahmet Hakan Argeşo, for their endless patience, continuous encouragement, valuable guidance, and inspiring ideas, which made the completion of this work possible. I feel extremely fortunate and privileged to have had their support, as they generously shared their knowledge and experience, guiding me both academically and professionally.

I would also like to extend my thanks to Asst. Prof. Dr. Ebru Akış, who, throughout the research process, provided invaluable insights and guidance. Her contributions shaped not only the academic aspect of this work but also greatly influenced my confidence and professional development. Her suggestions and perspectives were integral to my research journey.

I wish to thank my dear parents for always being there for me, no matter the circumstances. Their unwavering love and constant support have always been a source of strength and motivation for me. I would not have been able to reach this point without their unconditional support.

And last but not least, I want to thank my lifelong companion, Burak Şen, for always making me smile. His presence by my side in every step I took, his motivation, and his constant reminders to believe in myself made this journey far more meaningful, rewarding, and enjoyable.

TABLE OF CONTENTS

LIST OF TABLES

TABLE

LIST OF FIGURES

FIGURE

CHAPTER 1

INTRODUCTION

Functionally graded materials (FGMs) are considered as one of the new generations of composites which are made of two or more constituents of materials. The structural components made from FGMs are produced in such a way that the volumetric fraction of a constituent has a continuous gradual variation within the structural component. This process is called material gradation and reveals a microstructure that has continuous and steady variations of material and physical properties such as Young's modulus, density and coefficient of thermal expansion [1].

Generally, the structural components made of FGMs are designed to withstand extreme conditions. For example, one side of a structural component may resist high temperatures while the other side maintains its strong mechanical properties [2]. The structural elements made of FGMs are used especially in aerospace, automobile, defense, and biomedical industries. FGMs have been manufactured by different methods such as centrifugal casting and powder metallurgy [3].

FGMs have multifunctional properties with gradually changing material properties, and they are well-suited for engineering applications that require different properties in a structural component [4]. The properties of FGMs are based on volume fractions that contain gradient laws. Therefore, the thermal and mechanical analyses that will be performed on assemblies made of FGMs must be based on these gradient laws [5].

Analysis of the mechanical responses of structural assemblies made of FGMs have become an important topic for composite structures in recent years. Many studies have been carried out on the assemblies made of this composite under different loading and boundary conditions. The effect of temperature on the mechanical properties of these materials were also considered in the past.

In this chapter, some important studies on the relation between temperature and FGMs will be briefly summarized in three sections. In the first section, the related studies on the members made of temperature dependent homogenous materials will be given. In the second section, some key investigations on the structural components made of FGMs will be summarized. In the third section, the related studies in which the effect of temperature on FGMs will be given. Finally, in the last two sections, the scope of this study and the thesis organization will be given.

1.1 Temperature Dependent Material Properties

Thermal loads are caused by high temperatures, cyclic temperature changes, and other factors affecting mechanical and structural parts. It is a known fact that temperature affects the mechanical properties of materials significantly. At the environments that have high temperatures and/or high temperature changes, the analysis and design of structural elements without taking this fact into account may lead to substantial errors [6].

Duhamel [7] who developed the theory of thermal stresses and added the dilatation factor to the equation of thermal conductivity, was the first to propose a relation between deformation and temperature fields. This equation, though, lacked a solid thermodynamic foundation. Next, Voight [8] and Jeffreys [9] attempted to justify this equation using thermodynamics. The thermal conductivity equation was, however, fully justified in 1956 by Biot [10] using the thermodynamics of irreversible processes [11]. The essential techniques for resolving the thermoelasticity equation and the variational theorem were also introduced by Biot [12]. Problems related to the theory of thermal stresses were addressed by Melan and Parkus [13], Parkus [14], Boley and Weiner [15], and Nowacki [16].

In addition to all these, studies on thermal stresses in elastic and inelastic materials with temperature-dependent properties were investigated by several researchers in the past. Suhara in 1918 solved the thermoelastic response of a hollow circular cylinder in which the shear modulus depends on temperature [6,17].

The problem of transient thermoelasticity in a long circular cylinder with temperature dependent properties was solved by Koizumi and Taniwaki in 1965 [18]. The plane flexure and stability problem of a continuous thermal stress concentration around a thermally insulated circular hole in a plate under steady state condition was studied by El Karamani in 1978 [19]. The steady thermoelastic problem in a hollow cylinder was studied by Stanley and Chau in 1980 [20]. Noda and Daichyo presented a general solution strategy for the three-dimensional transient thermoelastic problems having temperature dependent properties [21-22].

The temperature-dependent properties of thermal parameters affected by thermal stress factors under constant volume were mentioned in Touloukian's publications [23-24]. It is known that Young's modulus, shear modulus, Poisson’s ratio, and coefficient of thermal expansion are the material parameters related to thermoelasticity. The Japan Society of Mechanical Engineers published a book in 1980 that included a list of the temperature dependences of these parameters [6].

Investigation of thermal stresses affected by temperature dependent properties for cylinders, tubes and disks has been the subject of several studies in the past. Gulgec and Orcan [25], presented the analytical solution of the elastic-plastic deformation of a free-ended heat-generating tube, considering the temperature dependence of the yield stress. Orcan and Eraslan [26], developed a model to determine the elastic-plastic behavior of internal heat-generating tubes with variable thermomechanical properties. Eraslan and Argeso [27], developed a computational model to determine elastic, elastic-plastic, fully plastic and residual stress states in axisymmetric structural members under generalized plane strain assumption considering temperature-dependent physical properties. They also conducted a parametric study to evaluate the effect of temperature dependency of physical properties on the thermomechanical response in heat-generating cylinders [28]. Zenkour and Abbas [29] investigated the effect of density and temperature-dependent material properties of an annular cylinder exposed to a thermal field. Abbas [30] also developed a general finite element model to analyze the thermoelastic response of a hollow cylinder considering temperature-dependent material properties.

1.2 Functionally Graded Materials

In 1972, the concept of structural gradients was initially introduced for the use in composites and polymeric materials [31,32]. For the gradients in composition, filament concentrations, and polymerization, several models were proposed, along with the potential uses for the resulting graded structures. But before the 1980s, not much research had been done on the fabrication, design, and evaluation of such structures [33].

FGMs were first introduced in 1984 at the National Aerospace Laboratory of Japan during a spaceflight project to prevent stress peaks at interfaces in coated panels for the space shuttle. The combination of materials used here was designed to maintain structural integrity in a thermal barrier system that can withstand a temperature gradient of 1000 K and a surface temperature of 2000 K across a 10 mm thick section [3,34,35]

In 1985, to improve the adhesion strength and reduce thermal stresses in the ceramic coatings and joints for the reusable rocket engine, continuous texture control was suggested [33]. These types of materials were first known as functionally gradient materials in 1986. The complete name was changed to functionally graded materials in 1995 due to a discussion during the Third International Symposium on FGMs, which took place in Lausanne in 1994. Extensive research was done on the design methods, theoretical modeling, processing, and evaluation of FGMs since they are inhomogeneous (heterogeneous) materials. Consequently, *Fundamental studies on the relaxation of thermal stress by tailoring graded structure,* a five-year research program, was started in Japan in 1987. The program's primary objective was to create FGMs that could withstand high temperatures in a hypersonic space plane [33,36].

An FGM is made from a combination of different material constituents, such as ceramic and metal, to provide thermal protection against large temperature changes. The most common FGM transitions from ceramic to metal is made by combining the properties of ceramics, such as heat, wear, and oxidation resistance, with the toughness, strength, machinability, and bonding capacity of metals, thereby reducing severe internal thermal stresses. The ceramic-rich surface provides thermal resistance, while the metal-rich surface provides structural strength and rigidity [37].

Since 1980's, FGM concepts have triggered research activities worldwide and have been applied to metal–metal, ceramic–ceramic or ceramic–polymer composites, in addition to ceramic–metal composites to produce advanced components with superior physical properties. Possible material combinations used in FGMs are shown in Figure 1.1 [38].

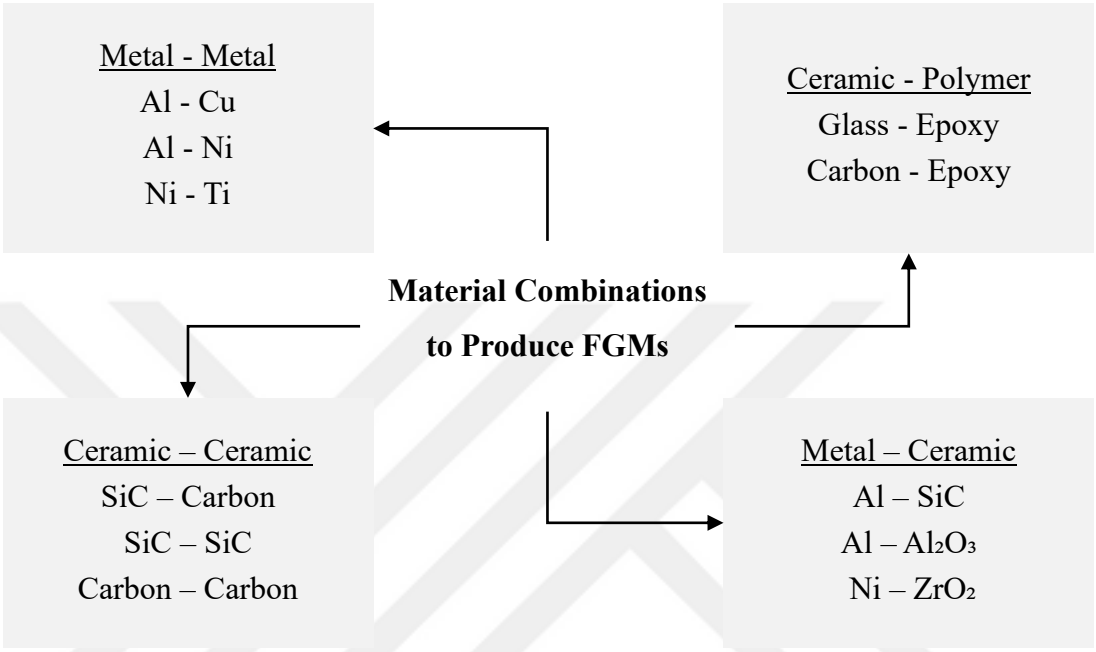

Figure 1.1: Possible material combinations of FGMs

FGMs enable the creation of new materials with special properties with the ability to combine incompatible functions. For example, FGMs can reduce interlayer stresses and prevent plastic deformation or cracking by appropriately grading the material components between interfaces in high-temperature applications such as thermal barrier coatings. They are widely adopted in various application fields of engineering and technology to take the advantage of the unique properties of existing materials. Various application areas of FGMs are shown in Figure 1.2 [33,35].

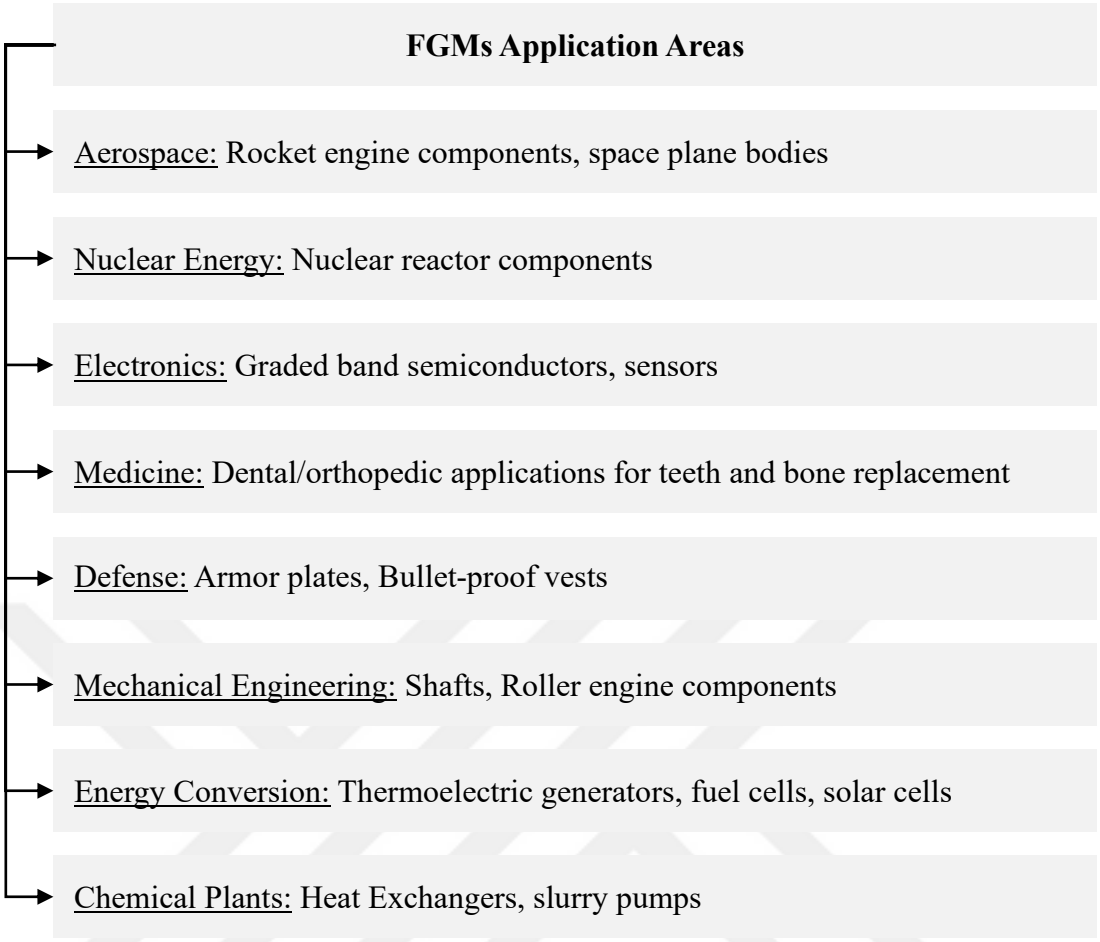

Figure 1.2: Various application areas of FGMs

Applications of FGMs are rapidly expanding as advancements in processing technology, production cost reductions, and improvements in material properties continue to drive innovation.

Material tailoring is the process of grading materials in accordance with intended needs. When using the appropriate material, structural components made of metal alloys or conventional composites can have better fracture toughness, improved thermal characteristics, and improved residual stress distributions. It should be noted that the interface problems between the fibers and the matrix that arise in conventional fiber-reinforced composites are also resolved by using FGMs [1].

Since there is a lack of precise information regarding the size, shape, and distribution of the particles in FGMs, the volume fraction distribution and the estimated shape of the dispersed phase are used to evaluate the effective elastic moduli of graded microstructures [39,40].

Figure 1.3 represents the profile of an FGM structural element made of two material constituents having two phases. As seen in this figure, the percentage variation in the volumetric proportion changes along the thickness direction. The percent volumetric fractions of material gradients A and B, represented by the yellow and red curves, respectively, are defined as V_A and V_B. Assuming that the elements are two different metal alloys, it is also shown that the volumetric percentage of the metallic phase resistant to mechanical loads decreases as it moves from the bottom to the upper surface, while the metallic phase resistant to high temperatures exhibits the opposite behavior. The components are arranged in a way that makes the upper part of the structure resistant to the high temperatures and the lower half to the mechanical loads.

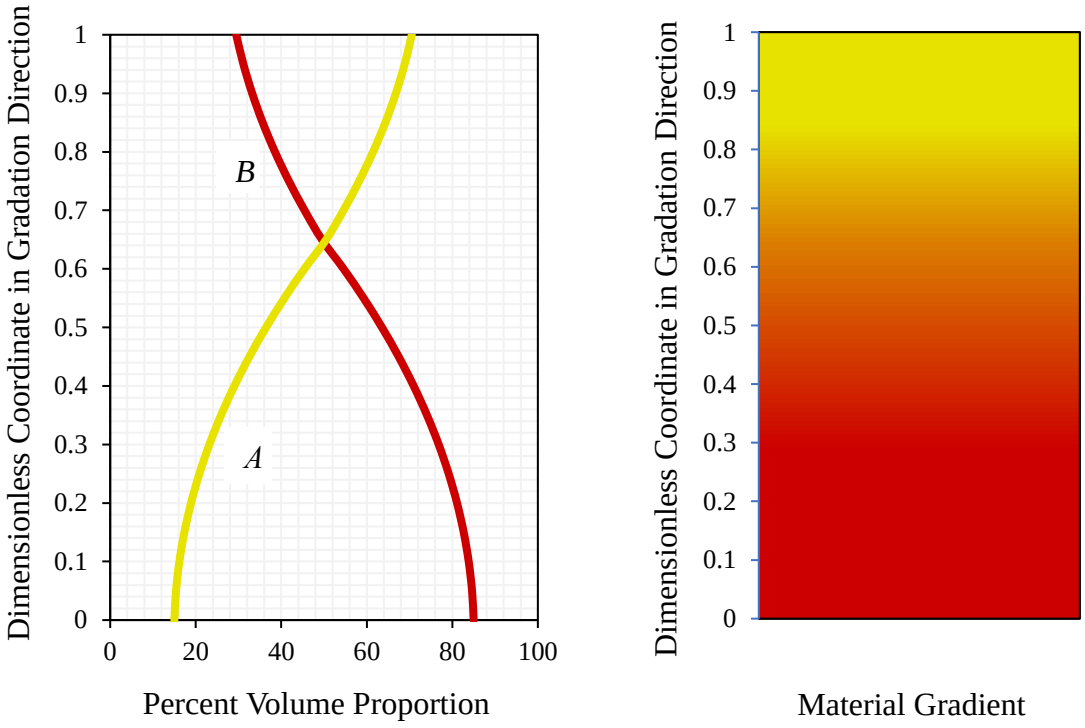

Figure 1.3: FGM variation in gradation direction

The linear elastic thermomechanical response of FGMs has been the subject of numerous investigations. Even though analytical methods provide closed-form solutions, they are only applicable to basic geometries, specific gradations of material properties (such as exponential or power law distribution), unique boundary and loading conditions. For example, Ying, Lu, and Chen [41] provided an exact solution for the bending and free vibration problems of functionally graded beams resting on a Winkler–Pasternak elastic foundation using the two-dimensional theory of elasticity. Peng and Li [42] analyzed the thermoelastic problem of a rotating functionally graded hollow circular disk. They introduced an analytical method to examine the steady thermal stresses in a functionally graded hollow circular disk rotating with a constant angular velocity around its central axis. Nie, Zhong, and Chen [43] obtained explicit solutions for specific through-the-thickness variations of Young's modulus, such as the exponential model, linear model, and reciprocal model for a beam made of FGM. Sankar and Tzeng [44] investigated thermal stresses in FGM beams where the thermoelastic constants and the temperature vary exponentially through the thickness, while the Poisson ratio is kept constant. Vel and Batra [45,46] presented solutions for three-dimensional thermomechanical deformations of a simply supported FGM rectangular plate under time-dependent thermal loads applied to its upper and/or lower surfaces. Ootao and Tanigawa [47] obtained an analytical solution to the transient thermoelastic problem associated with a multilayered hollow circular disk. In their work, the disc power law exhibited inhomogeneity and ensured equal heat supply from both internal and external surfaces. Ootao and Ishihara [48] presented the analytical solution of the transient thermoelastic problem for a FGM rectangular plate characterized by a piecewise exponential law subjected to a non-uniform heat source.

In some studies on the thermoelastic response of structural components made of FGMs, a finite element method was used. Among them, Nemat et al. [49] performed elastic–plastic stress analysis for two dimensional FGMs under thermal loads using the finite element method. Reddy and Chin [50] investigated the dynamic thermoelastic response of functionally graded plates and cylinders. Their formulation involved thermomechanical coupling, and a finite element model.

Praveen, Chin and Reddy [51] studied the pseudo-dynamic thermoelastic response of functionally graded ceramic-metal cylinders. They used the finite element formulation of the one-dimensional axisymmetric heat transfer equation in the solution of the thermoelastic radial boundary value problem. Wang and Mai [52] proposed a solution approach for the one-dimensional transient temperature and thermal stress fields. Explicit formulas were provided for one dimensional plates, rotationally symmetric spheres, and axially symmetric cylinders, where appropriate finite element formulations are used in their study. Ching and Chen [53] considered the thermophysical and thermomechanical properties that depend on temperature for both constituents in their study. Micromechanical models were used to assess the FGM's effective material properties. Darabseh, Yilmaz, and Bataineh [54] investigated the transient thermoelastic response of a thick hollow cylinder of FGM subjected to thermal loading. The theoretical framework of their study was based on the Green-Lindsay model and the equation of motion, and the heat conduction equation was solved using the Galerkin finite element method.

The concept of thermoelastic response of FGM hollow cylinders, tubes and spheres was investigated analytically and numerically by several researchers in the past. Liew et al. [55] investigated the thermomechanical behavior of hollow circular cylinders composed of FGMs. Zimmerman and Lutz [56] provided an exact solution to the problem of uniform heating of a cylinder, where Young's modulus and coefficient of thermal expansion varied linearly with radius. Tarn [57] obtained the temperature distribution, thermoelastic deformations, and stress responses within inhomogeneous hollow and solid cylinders. These cylinders demonstrated a power law dependence of the moduli. Shao et al. [58] performed thermo-mechanical analysis of FGM hollow circular cylinders under axisymmetric mechanical and transient thermal loads. It was assumed in their study that the thermo-mechanical properties of FGM remained independent of temperature and varied continuously in the radial direction of the hollow cylinder. Nejad and Rahimi [59] derived closed-form solutions for one-dimensional steady-state thermal stresses in a rotating FGM pressurized, thick-walled hollow circular cylinder using the small deformation theory.

Peng and Li [60] studied thermoelastic problems within a FGM hollow circular cylinder where material properties varied arbitrarily along the radial direction. A new and effective method was introduced in their work to determine the response of temperature and thermal stresses inside the cylinder. Jabbari et al. [61] performed a one dimensional steady-state thermal stress analysis in a thick, hollow cylinder composed of functionally graded material that was created in a generic way. It was assumed that the temperature distribution along the inner and outer surfaces was a function of the radius as well as the overall mechanical and thermal properties. Akis [62] examined the fully elastic, partially plastic, and fully plastic stress states in internally pressurized, functionally graded spherical pressure vessels using small deformation theory. It was assumed in his study that the elastic modulus and uniaxial yield limit of the material forming the spherical pressure vessel varied nonlinearly in the radial direction. In his other study [63] he investigated analytically the elastic behavior of a long tube made of a functionally graded material, generating internally nonuniform heat. It was assumed that the heat conduction coefficient and elastic modulus of the tube varied nonlinearly along the radial coordinate. Akis and Eraslan [64] presented the results of the elastic analysis of functionally graded cylindrical and spherical pressure vessels. Finally, Sharma and Kaur [65] numerically studied the stress field in a hollow cylinder made of FGM using the finite element method. FGM cylinder, thermoelastic material properties were assumed to vary exponentially along the radius of the cylinder.

1.3 Functionally Graded Materials and Temperature Dependency

To correctly simulate the mechanical and physical properties of FGMs, position and temperature dependency must be considered. This is achieved by computing the temperature-dependent properties of each parameter with rule of mixtures. The attributes of the constituents are generally expressed as functions of temperature, whereas the volume fraction, which represents the distribution of materials, is treated as a geometric function [50].

To analyze the temperature and position-dependent properties of FGMs, property profile gradient models, volume fraction gradient laws, and various assumptions which include volume fractions gradient laws and homogenization schemes have been made [5]. The research on the effects of temperature on the FGM assemblies were published in 1999 by Praveen et al. [51], followed by Wang and Mai [52], and by Wang and Tian [66] in 2005. The third study was based on a transient heat conduction problem for a one-dimensional strip, whereas the first two studies were focused on stresses in a one-dimensional axisymmetric hollow cylinder. Ching and Chen [53] examined the thermal stresses of FGMs with temperature-dependent properties and used the rule of mixtures (Voigt model) [39,40] to evaluate all effective temperature-dependent properties. It should be noted that the rule of mixtures may provide imprecise approximations for most effective properties since it ignores phase-to-phase contact. In some studies, micromechanics models or schemes have been proposed for the determination of temperature and position dependent properties of FGMs based on the Hill's self-consistent approach [67], Mori-Tanaka technique (Mori and Tanaka [68], Benveniste [69]) and Gibson equations [70].

Gradient laws describing the temperature-dependent properties of FGMs, geometric functions characterizing the position-dependent properties of FGMs, in other words the volume fractions gradient laws of components in FGMs, and homogenization micromechanics models and schemes containing the temperature and position dependent properties of FGMs constitute a wide scope of literature research. Shi, Xie and Li [5] published a detailed review paper covering these issues. In this important study, they summarized

(a) The gradient laws with numerical or analytical solutions that explain the properties of FGMs, such as power law, exponential law, linear law, general power law, general linear law, linear-power mixed law, exponential-power mixed law, power-linear law, polynomial law, and trigonometric law,
(b) The geometric functions for volume fractions gradient, such power law, sigmoidal law, and general power law,
(c) The homogenization schemes with different methods, such as estimate strategy, Voigt scheme, Reuss scheme, Mori-Tanaka scheme, Halpin-Tsai (HT) scheme, and Voigt-Reuss-Hill scheme.

1.4 Scope of the Study

Over the past years, extensive research has been conducted on heat transfer and thermal stress analyses of structural assemblies made of FGMs. The most important part of this concept is the determination of stresses in such assemblies, which play critical roles in the design of structural elements. FGMs have analytical complexity in performing heat transfer and thermal stress analyses. Closed form solutions are only obtained for selected cases with certain types of thermal loads, boundary conditions and material inhomogeneities. However, in line with the increasing demand for new structures and technologies, a better understanding of the thermal behavior and efficiency of FGMs has become important. Consequently, reliable, and efficient calculation methods are needed to evaluate the complex thermo-mechanical response of such structures at the design stage. Understanding the relevant concepts is important to ensure the integrity and performance of FGM in various practices. An effective method is always required to better understand how functionally graded materials (FGMs) behave in high-temperature environments and to predict heat transfer behavior and stresses.

In view of the above-mentioned facts, the thermal stresses in infinitely long circular tubes made of FGMs, which generates internal heat and with different thermal and mechanical boundary conditions, has been investigated in this study. In the analyses, a material grading function based on the error function, which varies in the radial direction and allows for a smooth and controlled grading of material properties, has been defined. The differential equations governing the thermal and mechanical problems have been numerically solved by using Mathematica [71]. Two sample problems having different thermal and mechanical loadings and boundary conditions are considered. For each problem, the distributions of field variables along the cross sections of the tubes are determined. The solutions determined for the tubes made of homogeneous materials that form the FGM tubes are compared with those obtained for the tubes made of functionally graded material.

1.5 Thesis Outline

The thesis is organized as follows: In Chapter 2, the problem definition and the formulation are introduced for the thermoelastic analysis of FGM infinitely long circular tubes that have internal heat generation. In Chapter 3, FGM properties are determined, considering the position and temperature dependencies. The error function that is used to define the material gradation is also introduced in this chapter. In Chapter 4, numerical results obtained by the solutions to the two sample problems are presented. Finally, in Chapter 5, some conclusions are given.

CHAPTER 2

PROBLEM DEFINITION

2.1 Introduction

In this study, thermoelastic response of an internally heat generating functionally graded infinitely long thick-walled circular tube is investigated. The two ends of the tube are assumed to be axially constrained (fixed ends) and subjected to axisymmetric thermal and mechanical loading. In the formulation of the mechanical problem, a state of plane strain and small deformation theory are assumed. In addition, cylindrical coordinate system is used in the formulations. The directions of cylindrical coordinates and the corresponding stress components in the thick-walled circular tube are shown in Figure 2.1

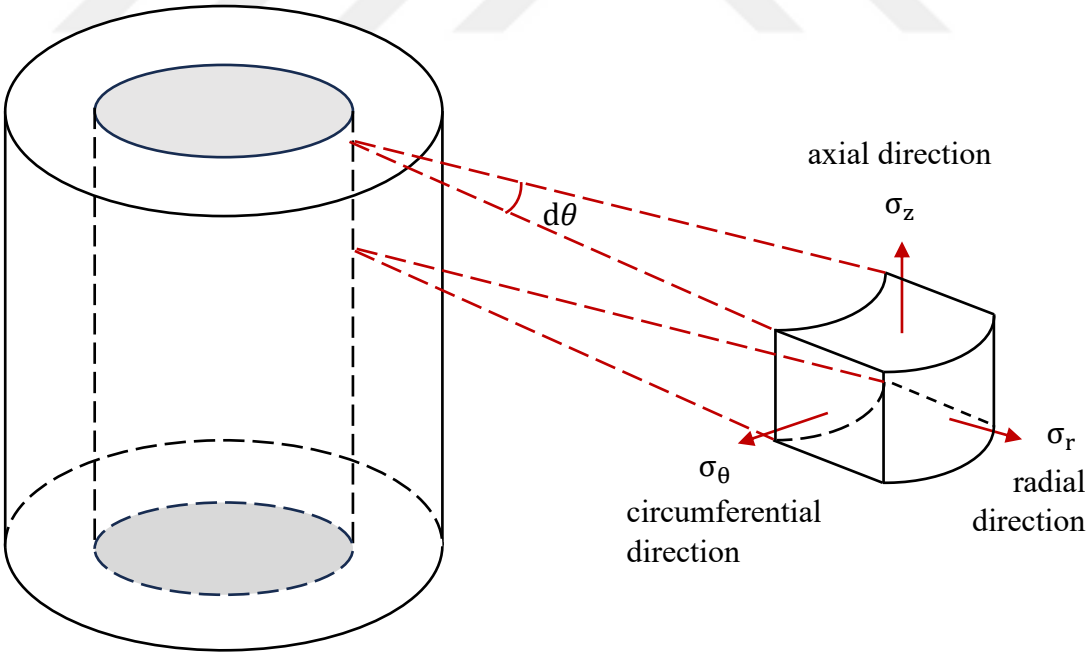

Figure 2.1: Cylindrical coordinates and stress components in the thick-walled circular tube

The cross-section of the tube is shown in Fig. 2.2. The inner and outer radii of the tube are defined as a and b, respectively. It is assumed that the tube is made of an FGM with gradation along radial direction and the material properties are temperature dependent.

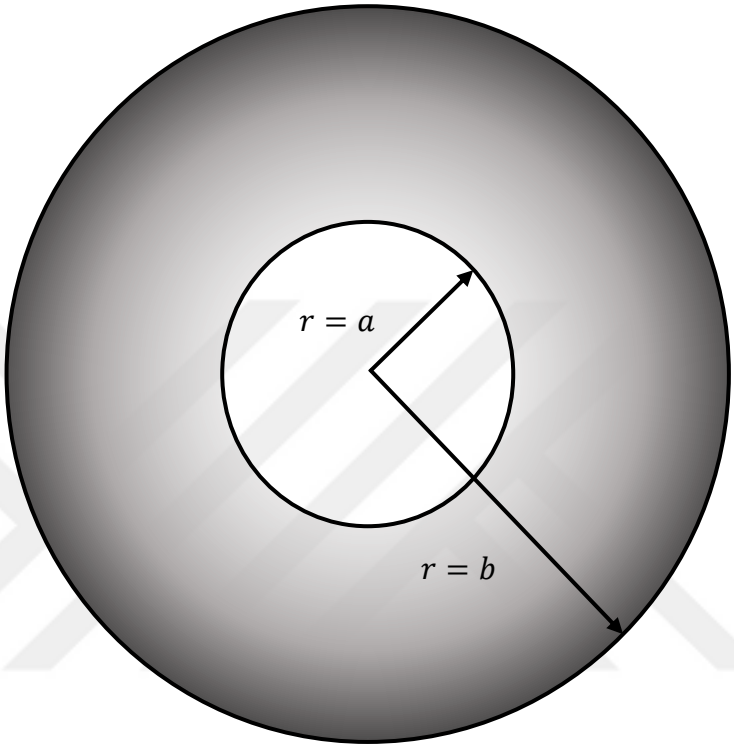

Figure 2.2: Cross section of functionally graded circular tube

In the formulations, all the material properties are assumed to be functions of radial coordinate and temperature as seen in Eq. (2.1).

$$\begin{aligned} &k = k(r,T) \;\; ; \;\; \alpha = \alpha(r,T) \quad ; \;\; E = E(r,T) \\ &\nu = \nu(r,T) \;\; ; \;\; \sigma_u = \sigma_u(r,T) \;\; ; \;\; \rho = \rho(r,T) \end{aligned} \tag{2.1}$$

Here, k is the thermal conductivity, α is the thermal expansion coefficient, E is the modulus of elasticity, ν is the Poisson's ratio, σ_u is the uniaxial yield limit and ρ is the density.

It should be noted that when the temperature distribution T is obtained after the solution of the thermal problem, the material properties will be functions of radial coordinate r. In another words, if M represents any material property which is a function of radial coordinate and temperature $M = M(r,T)$ and if the temperature distribution is obtained as $T = T(r)$, we will have the material property $M = M(r)$ in the end.

In the next section, the definition of the thermal problem will be presented.

2.2 Definition of the Thermal Problem

The tube under consideration is assumed to be in steady-state condition and axisymmetric. The governing energy equation under these assumptions becomes [15,72]

$$\frac{\mathrm{d}}{\mathrm{d}r}\left(k(r,T)\,\frac{\mathrm{d}T}{\mathrm{d}r}\right)+\frac{k(r,T)}{r}\frac{\mathrm{d}T}{\mathrm{d}r}+Q(r)=0 \tag{2.2}$$

where $Q = Q(r)$ is the axisymmetric internal heat generation. By taking the derivate in the first term and rearranging one obtains

$$k(r,T)\frac{\mathrm{d}^2T}{\mathrm{d}r^2}+\left(\frac{k(r,T)}{r}+\frac{\partial}{\partial r}k(r,T)\right)\frac{\mathrm{d}T}{\mathrm{d}r}+\frac{\partial}{\partial T}k(r,T)\left(\frac{\mathrm{d}T}{\mathrm{d}r}\right)^2+Q(r)=0 \tag{2.3}$$

Eq. (2.3) is a second order nonlinear ordinary differential equation (ODE) that governs the thermal problem. For the thermal boundary conditions (BC's), either (a) a prescribed temperature, or (b) an insulated surface is considered. These BC's for the inner surface (at $r = a$) can be expressed as

Prescribed temperature: $T(a) = T_{\mathrm{in}}$ (2.4a)

Insulated surface: $\left.\frac{\mathrm{d}T}{\mathrm{d}r}\right|_{r=a} = 0$ (2.4b)

Similarly, for the outer surface (at $r = b$)

Prescribed temperature: $T(b) = T_{out}$ (2.5a)

Insulated surface: $\left.\frac{\mathrm{d}T}{\mathrm{d}r}\right|_{r=\mathrm{b}} = 0$ (2.5b)

Eq. (2.3) and one BC described for each surface (inner and outer) constitutes the boundary value problem (BVP) of the thermal problem in the study.

2.3 Definition of the Mechanical Problem

Following the notation of [15] the only nonzero strain components are the normal strain components along radial and circumferential directions which are, respectively, ε_r and ε_θ. The axial strain component $\varepsilon_z = 0$ since we assume the ends of the tube are fixed. The strain-displacement relations in cylindrical coordinate system are given as

$$\varepsilon_r = \frac{\mathrm{d}u}{\mathrm{d}r} \tag{2.6}$$

$$\varepsilon_\theta = \frac{u}{r} \tag{2.7}$$

In Eqs. (2.6) and (2.7) u is the radial displacement, and it is the only non-zero displacement component for the problem under consideration. Using Eqs. (2.6) and (2.7), the compatibility relationship can be written as

$$\frac{\mathrm{d}}{\mathrm{d}r}(r\varepsilon_\theta) - \varepsilon_r = 0 \tag{2.8}$$

On the other hand, the equation of equilibrium in radial direction is given by

$$\frac{\mathrm{d}\sigma_r}{\mathrm{d}r} + \frac{\sigma_r - \sigma_\theta}{\mathrm{d}r} = 0 \tag{2.9}$$

The equations of the generalized Hooke's law relating strains to stresses are

$$\varepsilon_r = \frac{1}{E(r)}[\sigma_r - \nu(r)(\sigma_\theta + \sigma_z)] + G(r) \tag{2.10}$$

$$\varepsilon_\theta = \frac{1}{E(r)}[\sigma_\theta - \nu(r)(\sigma_r + \sigma_z)] + G(r) \tag{2.11}$$

$$\varepsilon_z = \frac{1}{E(r)}[\sigma_z - \nu(r)(\sigma_r + \sigma_\theta)] + G(r) \ = 0 \tag{2.12}$$

where the $G(r)$ is the function given by,

$$G(r) \ = \int_{T_0}^{T(r)} \alpha(r,\xi)\mathrm{d}\xi \tag{2.13}$$

with T_0 being the reference temperature. Here, thermal expansion coefficient is expressed by using the form $\alpha = \alpha(r, T(r))$. The material constants $E(r)$ and $\nu(r)$ are considered to be functions of r since the temperature distribution $T(r)$ is assumed to be determined after the solution of the thermal problem.

It should also be noted that σ_z can be written in terms of σ_r, σ_θ and $G(r)$ as

$$\sigma_z = \nu(r)(\sigma_r + \sigma_\theta) - E(r)G(r) \tag{2.14}$$

Herein, a stress function $Y(r)$ is introduced as

$$Y(r) = r\sigma_r \tag{2.15}$$

therefrom

$$\sigma_r = \frac{Y(r)}{r} \tag{2.16}$$

Inserting Eq. (2.16) into equation of equilibrium (Eq. (2.9)) yields

$$\sigma_\theta = \frac{\mathrm{d}Y}{\mathrm{d}r} \tag{2.17}$$

Using Eqs. (2.15), (2.16) and (2.17), σ_z can be written as

$$\sigma_z = \nu(r)\left(\frac{Y(r)}{r} + \frac{\mathrm{d}Y}{\mathrm{d}r}\right) - E(r)G(r) \tag{2.18}$$

The strain components ε_r and ε_θ can be expressed in terms of stress function with the use of Eqs. (2.10) and (2.11) together with Eq. (2.14). The result is

$$\varepsilon_r = \frac{1}{E(r)}\left[\frac{(1-\nu(r)^2)}{r}Y(r) - \nu(r)\big(1+\nu(r)\big)\frac{\mathrm{d}Y}{\mathrm{d}r}\right] + \big(1+\nu(r)\big)G(r) \tag{2.19}$$

$$\varepsilon_\theta = -\frac{1}{E(r)}\left[\frac{\nu(r)\big(1+\nu(r)\big)}{r}Y(r) - (1-\nu(r)^2)\frac{\mathrm{d}Y}{\mathrm{d}r}\right] + (1+\nu(r))G(r) \tag{2.20}$$

Finally, substituting Eqs. (2.19) and (2.20) into compatibility equation (Eq. (2.8)) yields

$$\begin{aligned}&\frac{\mathrm{d}^2Y}{\mathrm{d}r^2} + \left[\frac{1}{r} - \frac{1}{E(r)}\frac{\mathrm{d}E}{\mathrm{d}r} - \frac{2\nu(r)}{(1-\nu(r)^2)}\frac{\mathrm{d}\nu}{\mathrm{d}r}\right]\frac{\mathrm{d}Y}{\mathrm{d}r}\\ &-\left[\frac{1}{r} - \frac{\nu(r)}{E(r)\big(1-\nu(r)\big)}\frac{\mathrm{d}E}{\mathrm{d}r} + \frac{1+2\nu(r)}{(1-\nu(r)^2)}\frac{\mathrm{d}\nu}{\mathrm{d}r}\right]\frac{Y(r)}{r}\\ &= -\frac{E(r)}{(1-\nu(r)^2)}\left[\big(1+\nu(r)\big)\frac{\mathrm{d}G}{\mathrm{d}r} + G(r)\frac{\mathrm{d}\nu}{\mathrm{d}r}\right]\end{aligned} \tag{2.21}$$

Equation (2.21) is the thermoelastic equation expressed in terms of stress function $Y(r)$ which governs the mechanical problem.

Two different types of mechanical BC's are considered in the study. We consider either (a) a prescribed displacement, or (b) a prescribed radial stress. These are expressed for inner surface (at $r = a$) as

Prescribed displacement: $u(a) = u_{\text{in}}$ (2.22a)

Prescribed radial stress: $\sigma_r(a) = (\sigma_r)_{\text{in}}$ (2.22b)

Similarly, for the outer surface (at $r = b$)

Prescribed displacement: $u(b) = u_{\text{out}}$ (2.23a)

Prescribed radial stress: $\sigma_r(b) = (\sigma_r)_{\text{out}}$ (2.23b)

Since the thermoelastic equation is given in terms of stress function $Y(r)$, the mechanical BC's should also be expressed in terms of $Y(r)$. In the case of prescribed radial displacements at the inner and outer surfaces, we first note $u = r\varepsilon_\theta$ from Eq. (2.7) and then write it at $r = a$ and at $r = b$. These yields

$$u(a) = u_{\text{in}} = H_1(a)Y(a) + H_2(a)\left.\frac{\mathrm{d}Y}{\mathrm{d}r}\right|_{r=a} + H_3(a) \tag{2.24a}$$

$$u(b) = u_{\text{out}} = H_1(b)Y(b) + H_2(b)\left.\frac{\mathrm{d}Y}{\mathrm{d}r}\right|_{r=b} + H_3(b) \tag{2.24b}$$

for the prescribed displacements at the inner and outer surfaces, respectively. Here, the functions $H_1(r)$, $H_2(r)$ and $H_3(r)$ are defined as

$$H_1(r) = -\frac{\nu(r)(1+\nu(r))}{E(r)} \tag{2.25a}$$

$$H_2(r) = \frac{r(1-\nu(r)^2)}{E(r)} \tag{2.25b}$$

$$H_3(r) = r(1+\nu(r))\,G(r) \tag{2.25c}$$

In the case of prescribed radial stresses, the definition of $Y(r)$ from Eq. (2.15) is used. Writing it at $r = a$ and at $r = b$ yields

$$Y(a) = a\sigma_{\mathrm{r}}(a) = a(\sigma_r)_{\mathrm{in}} \tag{2.26a}$$

$$Y(b) = b\sigma_{\mathrm{r}}(b) = b(\sigma_r)_{\mathrm{out}} \tag{2.26b}$$

for the prescribed radial stresses for the inner and outer surfaces, respectively.

CHAPTER 3

MATERIAL MODELING

3.1 Position Dependency

Many FGMs are produced from two different constituents having different properties and in general, a detailed description of true microstructures of an FGM is not easy to determine. On the other hand, the information on the volumetric fraction distribution of any constituent, that is the volume ratio of the constituent to the total volume, can be determined. These fractions are expressed as decimals between 0 and 1. For example, if a constituent at a point inside the FGM structure has a 50% volume content then volume fraction is expressed as 0.5. Since the volume fractions of each constituent gradually change in the direction of gradation, the effective properties of FGMs change in the same direction. The volume fractions of all constituent materials should add up to unity [39], which can be formulated as

$$\sum_{i=1}^{n} V_i = 1 \tag{3.1}$$

where V_i is the volume fraction of the constituent material i, and n is the total number of different constituents that form the FGM.

As stated before, the volume fractions are decimals between 0 and 1. For example, if an FGM is formed from 3 constituents we have

$$V_1 + V_2 + V_3 = 1 \tag{3.2}$$

It should be noted that Eq. (3.2) must be satisfied at every point inside the domain of structural element made by FGM.

In this study, we assume that FGM is formed from two different constituents. We also recall that the FGM is graded along the radial direction of the tube. Denoting the volumetric fractions of the first and second constituents by $V_1 = V_1(r)$ and $V_2 = V_2(r)$, respectively, we have

$$V_1(r) + V_2(r) = 1 \tag{3.3}$$

considering the rule of mixtures [39,40].

Since we have two constituents, specifying the volumetric fraction of one of constituents is sufficient to completely describe the gradation of FGM. For example, if the volumetric fraction of the first constituent $V_1(r)$ is specified then from the rule of mixtures (Eq. (3.3)), the volumetric fraction of the second constituent will become $V_2(r) = 1 - V_1(r)$. Therefore, from this point, we only specify the volumetric fraction of the first constituent.

In this study, a gradation function based on error function is used to define the variation along radial direction, in which a smooth and controlled gradation of the constituents will be possible.

3.1.1 Error Function

A brief information about the properties and behavior of error function will be presented at the beginning. Then, the variation of material properties using error function will be introduced.

The error function, denoted as $erf(z)$, is defined as the integral of the Gaussian distribution [73] and is given by

$$\mathrm{erf}(r) = \frac{2}{\sqrt{\pi}} \int_0^r \mathrm{e}^{-t^2}\, \mathrm{d}t \tag{3.4}$$

The plot of $\mathrm{erf}(r)$ is shown in Fig. 3.1.

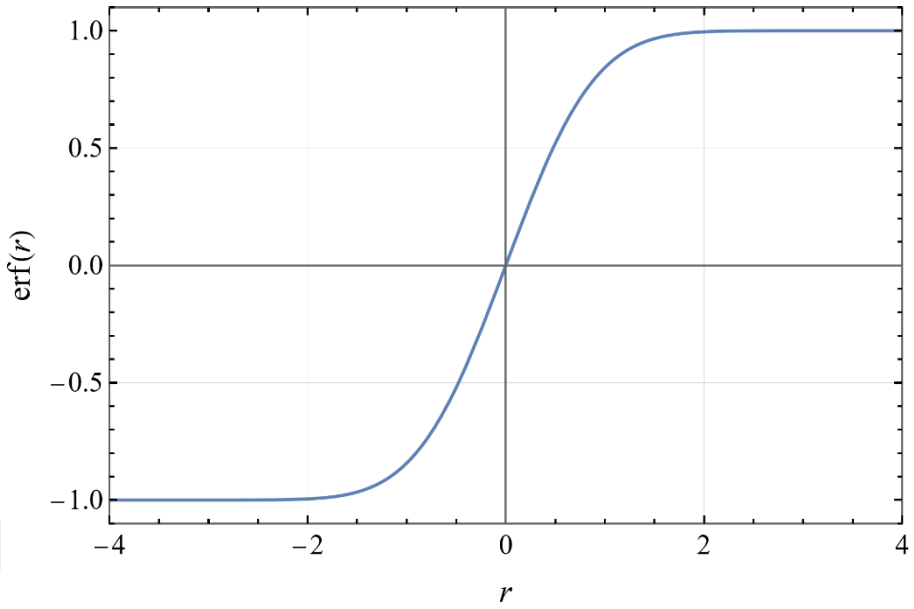

Figure 3.1: Error function $\mathrm{erf}(r)$

As seen from this figure, the range of $\mathrm{erf}(r)$ is between -1 and 1. It should be noted that

$$\mathrm{erf}(0) = 0, \lim_{r\to-\infty} \mathrm{erf}(r) = -1, \text{and } \lim_{r\to\infty} \mathrm{erf}\,(r) = 1 \tag{3.5}$$

where $r = 0$ is the inflection point for $\mathrm{erf}\,(r)$.

The derivative of $\mathrm{erf}(r)$ with respect to r is

$$\frac{\mathrm{d}}{\mathrm{d}r}\,[\mathrm{erf}(r)] = \frac{2}{\sqrt{\pi}}\mathrm{e}^{-r^2} \tag{3.6}$$

and one may show that it is an even function.

The plot of derivative of erf(r) is given in Fig. 3.2.

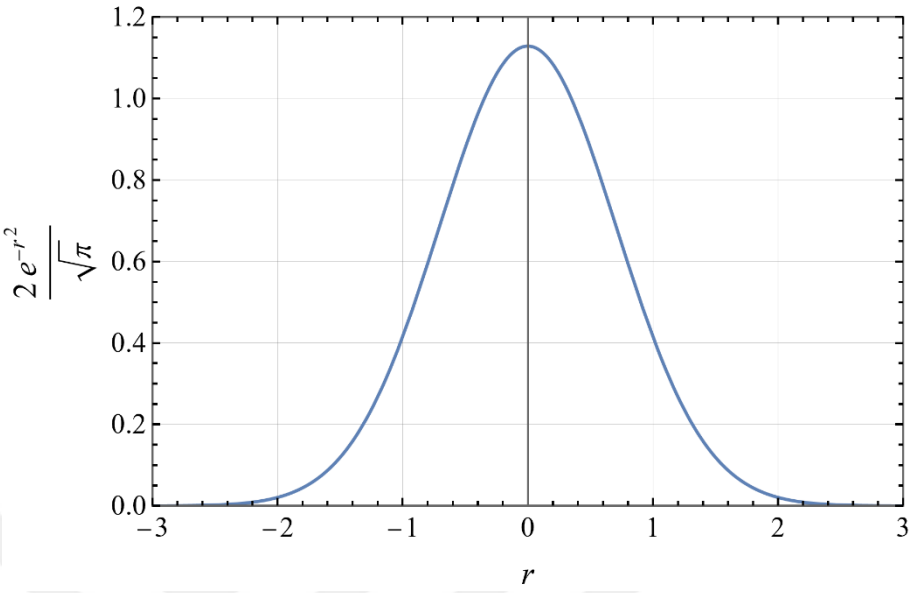

Figure 3.2: Plot of derivative of error function

At $r = 0$, we have

$$\frac{\mathrm{d}}{\mathrm{d}r}\,[\mathrm{erf}(r)]\Big|_{r=0} = \frac{2}{\sqrt{\pi}} \tag{3.7}$$

and as r goes to $-\infty$ and ∞ $\mathrm{d}\,[\mathrm{erf}(r)]/\mathrm{d}r$ approaches to 0.

The inverse of error function, denoted by erf^{-1}, and the plot of $\text{erf}^{-1}(r)$ is shown in Fig. 3.3.

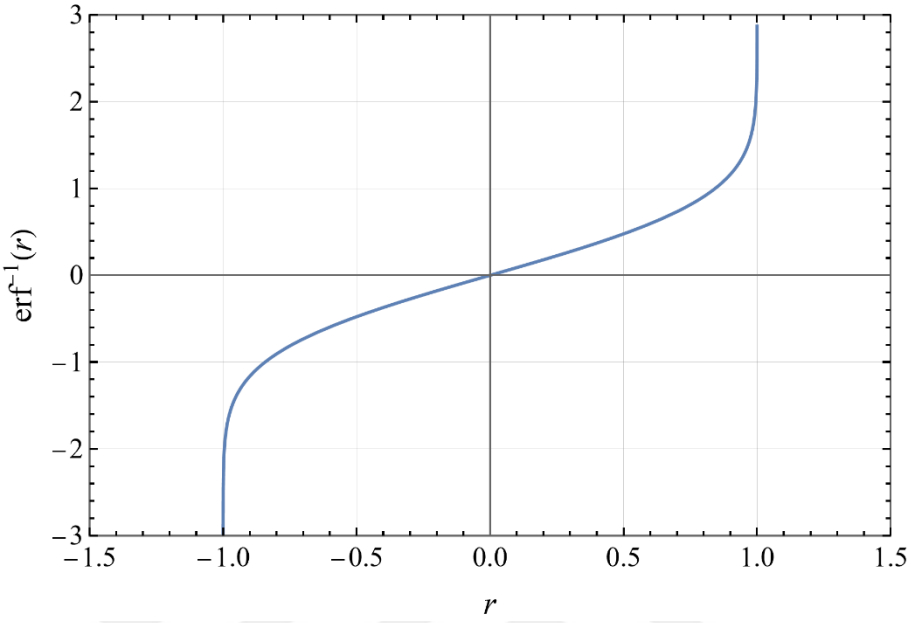

Figure 3.3: Plot of $\text{erf}^{-1}(r)$

As seen from this figure, its domain is $-1 \leq \text{erf}^{-1}(r) \leq 1$. Note that

$$\text{erf}^{-1}(0) = 0, \lim_{r\to-1} \text{erf}^{-1}(r) = -\infty, \text{and} \lim_{r\to1} \text{erf}^{-1}(r) = \infty \tag{3.8}$$

It should also be noted that

$$\text{erf}\big(\text{erf}^{-1}(r)\big) = r \text{ and } \text{erf}^{-1}\big(\text{erf}(r)\big) = r \tag{3.9}$$

Next, we consider the function $\text{erf}(m\,r)$ where m is a real valued parameter. Figures 3.4 and 3.5 show the variations of $\text{erf}(m\,r)$ plotted for various m values, whose signs are positive and negative, respectively.

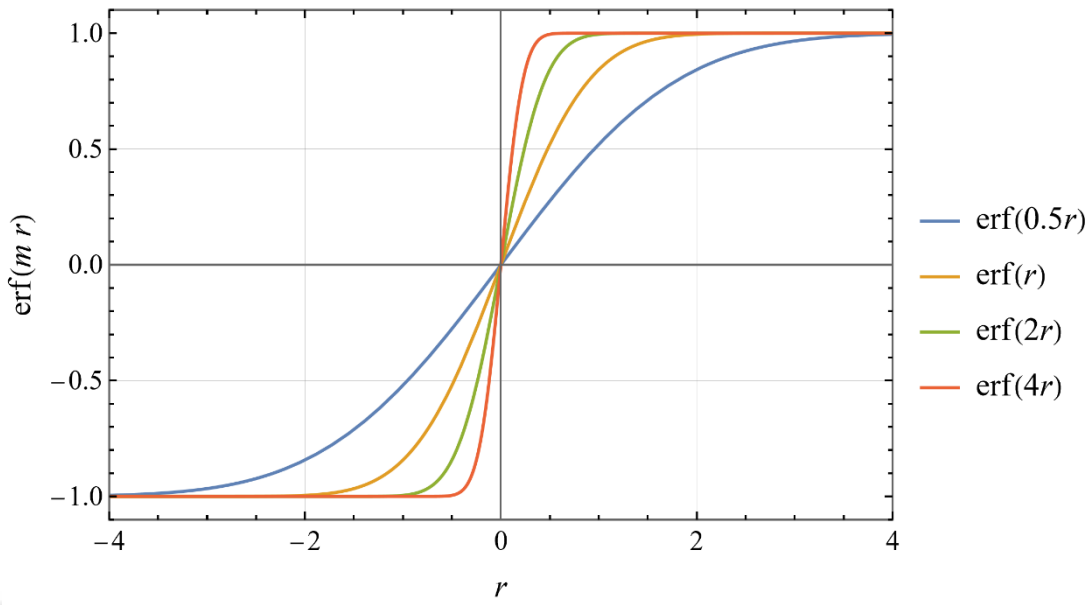

Figure 3.4: Plot of erf$(m\,r)$ for $m = 0.5, 1, 2,$ and 4

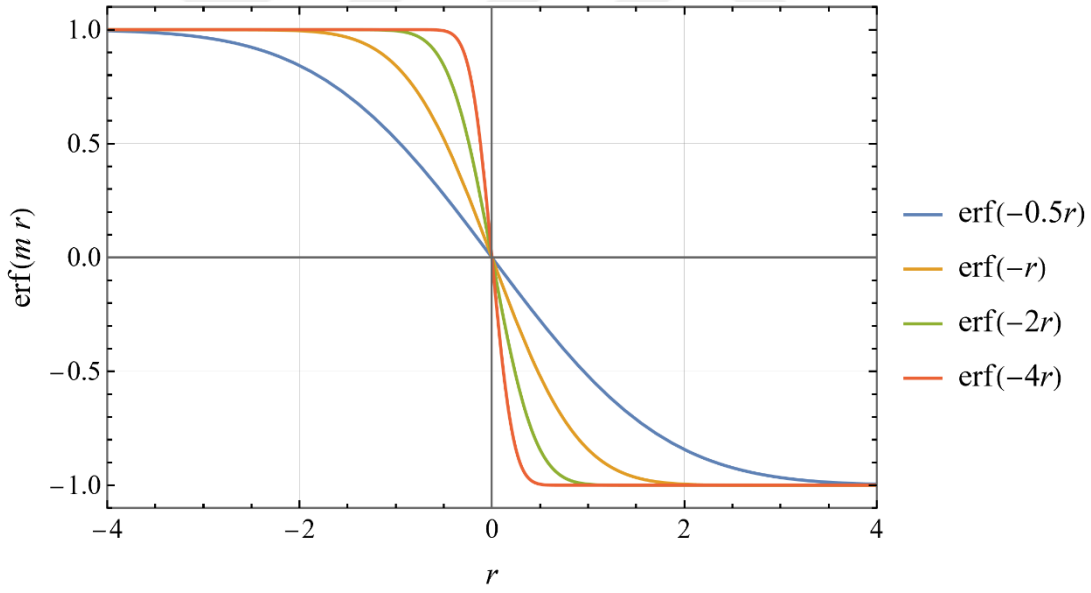

Figure 3.5: Plot of erf$(m\,r)$ for $m = -0.5, -1, -2,$ and -4

From Figs 3.4 and 3.5 we observe that as $|m|$ increases, the gradient of erf$(m\,r)$ increases. For the positive values of m, erf$(m\,r)$ varies from -1 to 1 as r increases, whereas, for negative values of m we have a variation from 1 to -1 as r increases.

To set an appropriate value of m to achieve a desired variation, we make use of the following equation.

$$\text{erf}(m\, r_{cr}) = p_{cr} \tag{3.10}$$

The graph of $\text{erf}(m\, r)$ is presented in Fig. 3.6.

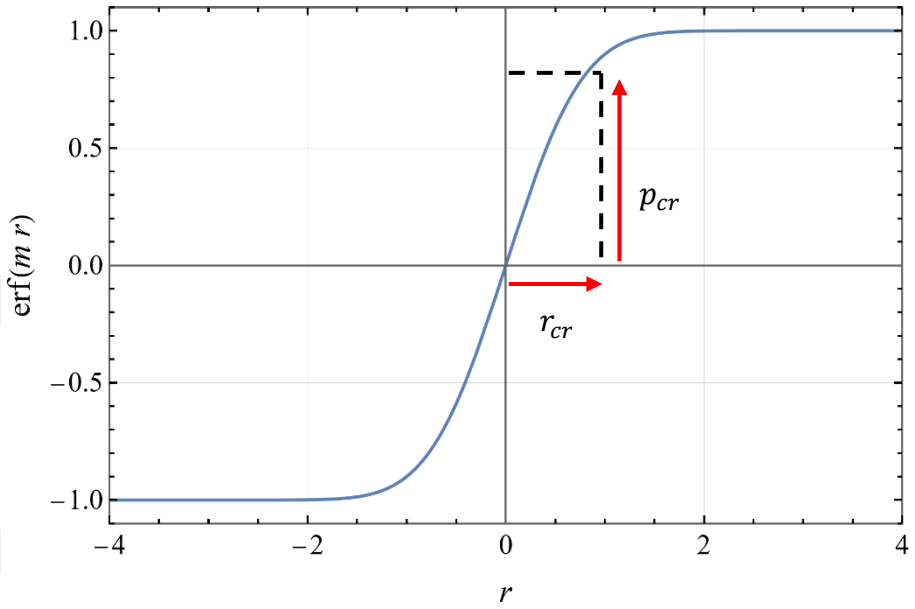

Figure 3.6: Plot of the function $\text{erf}(m\, r)$, r_{cr} and p_{cr}

Referring to Fig. 3.6, it is seen that r_{cr} is the distance from $r = 0$ to the point where $\text{erf}(m\, r)$ becomes p_{cr}. By prespecifying p_{cr} and r_{cr} values, one may easily control the desired variation.

After setting these two parameters (p_{cr} and r_{cr}), m is determined by making the use of inverse error function. For this, we write $m\, r_{cr} = \text{erf}^{-1}(p_{cr})$ first, then obtain m as

$$m = \frac{\text{erf}^{-1}(p_{cr})}{r_{cr}} \tag{3.11}$$

We see that as r_{cr} increases, the gradient of erf$(m\, r)$ decreases. It should be noted that, p_{cr} must be given such that $0 < p_{cr} < 1$. The value of p_{cr} designates the total percent variation of erf$(m\, r)$ that is achieved between -1 to 1 within the interval $-r_{cr} < r < r_{cr}$. Fig. 3.7 depicts the variations of erf$(m\, r)$ for $p_{cr} = 0.9$ and $r_{cr} = 1,2$ and 3. The corresponding values for m, which are calculated using Eq. (3.11) are $m = 1.1631, 0.5815$ and 0.3877.

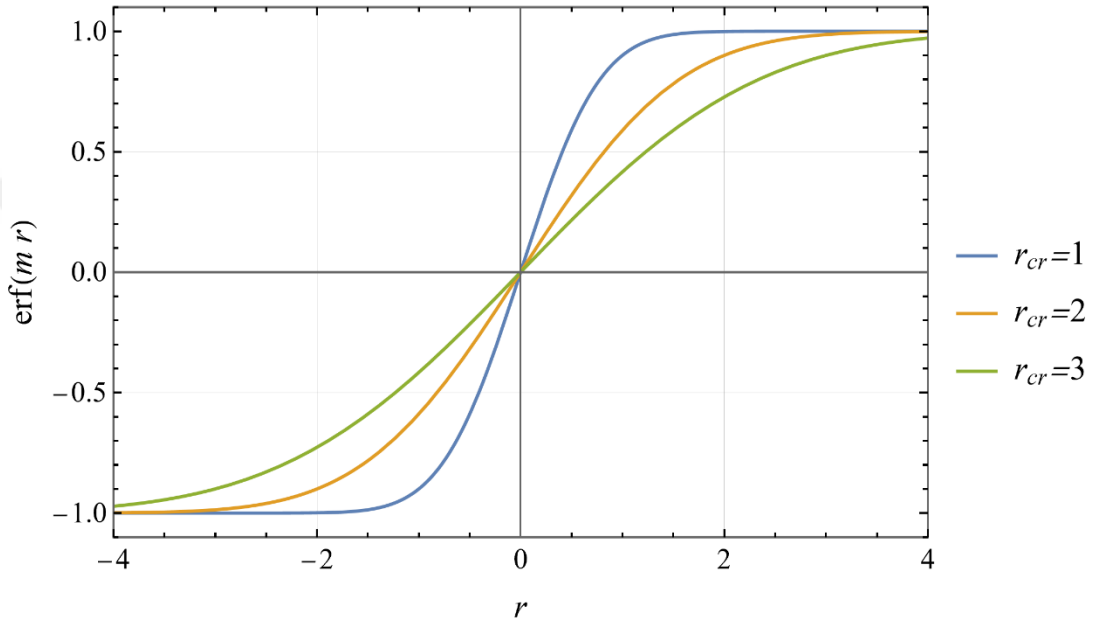

Figure 3.7: Plots of the function erf$(m\, r)$ for $p_{cr} = 0.9$ and $r_{cr} = 1,2,$ and 3

At this point, we introduce the proposed variation function. The volumetric fraction of the first constituent is given by

$$V_1(r) = s_1 + s_2 \text{erf}\left(m(r - r_{ip})\right) \tag{3.12}$$

In Eq. (3.12), r_{ip} is the inflection point of the variation, parameter m is used to control the gradient of $V_1(r)$ which is given by the Eq. (3.12), s_1 and s_2 are the parameters, respectively, for shifting and scaling of the function which serve to arrange the variation of $V_1(r)$ such that $a \leq r \leq b$ and $0 \leq V_1(r) \leq 1$. It should be noted, a and b are the inner and outer radii of the tube.

The values of s_1 and s_2 are related to the volumetric fraction values at the inner and outer values of the tube by

$$s_1 = \frac{V_1(a) + V_1(b)}{2} \tag{3.13a}$$

$$s_2 = \frac{V_1(b) - V_1(a)}{2} \tag{3.13b}$$

We note that, in Eq. (3.11), m can be decreased to reduce the rate of volume change, and p_{cr} can be reduced or r_{cr} can be increased to reduce m.

Figure 3.8 shows five different variations of $V_1(r)$, when $V_1(a) = 0.0$, $V_1(b) = 1.0$ and $r_{ip} = 0.3$. Using Eq. (3.13), we may calculate $s_1 = 0.5$ and $s_2 = 0.5$. These five variations are plotted for $r_{cr} = 0.02, 0.04, 0.06, 0.08,$ and 0.1. The m values are computed from Eq. (3.11) by preselecting $p_{cr} = 0.9$ as $m = 58.1544, 29.0772, 19.3848, 14.5386,$ and 11.6309. As seen from this figure, $V_1(r)$ changes from 0 to 1 as r increases, and it has an inflection point at $r_{ip} = 0.3$. It should also be noted that r_{cr} increases, the gradient of $V_1(r)$ decreases.

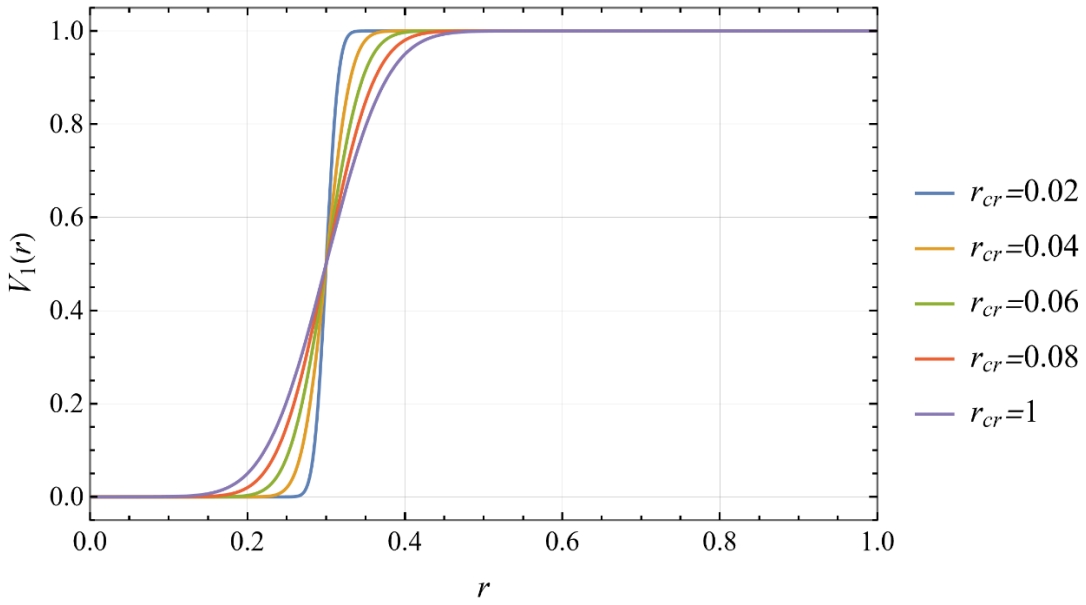

Figure 3.8: Variation of $V_1(r)$ for $r_{cr} = 0.02, 0.04, 0.06, 0.08,$ and 0.1, $r_{ip} = 0.3$, $s_1 = 0.5$, $s_2 = 0.5$ and $p_{cr} = 0.9$

By only changing the sign of s_2, setting it to be -0.5 and taking all the remaining parameters as the same as in the previous example, we reverse the behavior of $V_1(r)$ such that this time it changes from 1 to 0 as r increases. This can also be verified by letting $V_1(a) = 1.0, V_1(b) = 0.0$ and using Eq. (3.13), which yields $s_1 = 0.5$ and $s_2 = -0.5$.

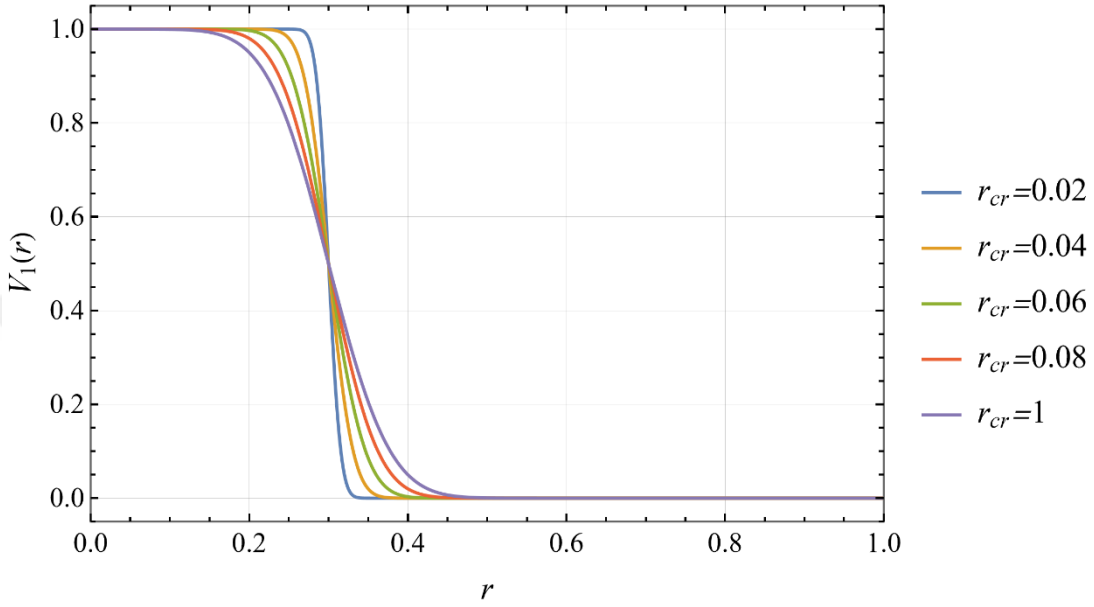

Figure 3.9: Variation of $V_1(r)$ for $r_{cr} = 0.02, 0.04, 0.06, 0.08$, and 0.1, $r_{ip} = 0.3$, $s_1 = 0.5$, $s_2 = -0.5$ and $p_{cr} = 0.9$

Figure 3.10 shows the variations of $V_1(r)$ in the case $V_1(a) = 0.6$, $V_1(b) = 1.0$ and $r_{ip} = 0.3$. For this case, we have $s_1 = 0.8$ and $s_2 = 0.2$. The p_{cr} value and r_{cr} values are selected to be the same as in the previous examples.

The reverse behavior can be obtained by changing the sign of s_2 and setting it to be $s_2 = -0.2$. This case is shown in Figure 3.11.

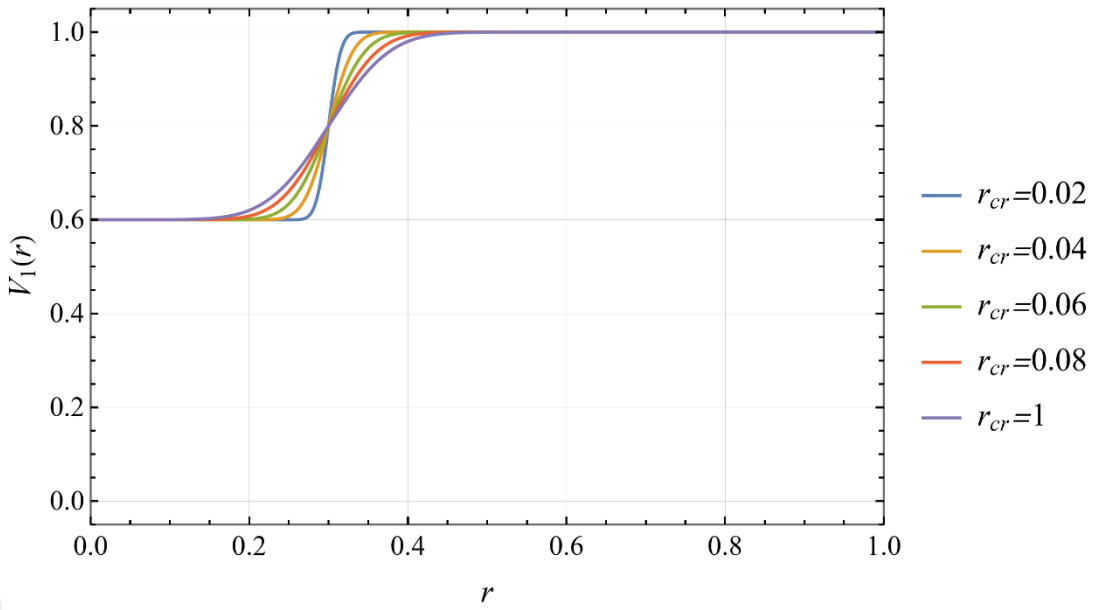

Figure 3.10: Variation of $V_1(r)$ for $r_{cr} = 0.02, 0.04, 0.06, 0.08,$ and 0.1, $r_{ip} = 0.3$, $s_1 = 0.8$, $s_2 = 0.2$ and $p_{cr} = 0.9$

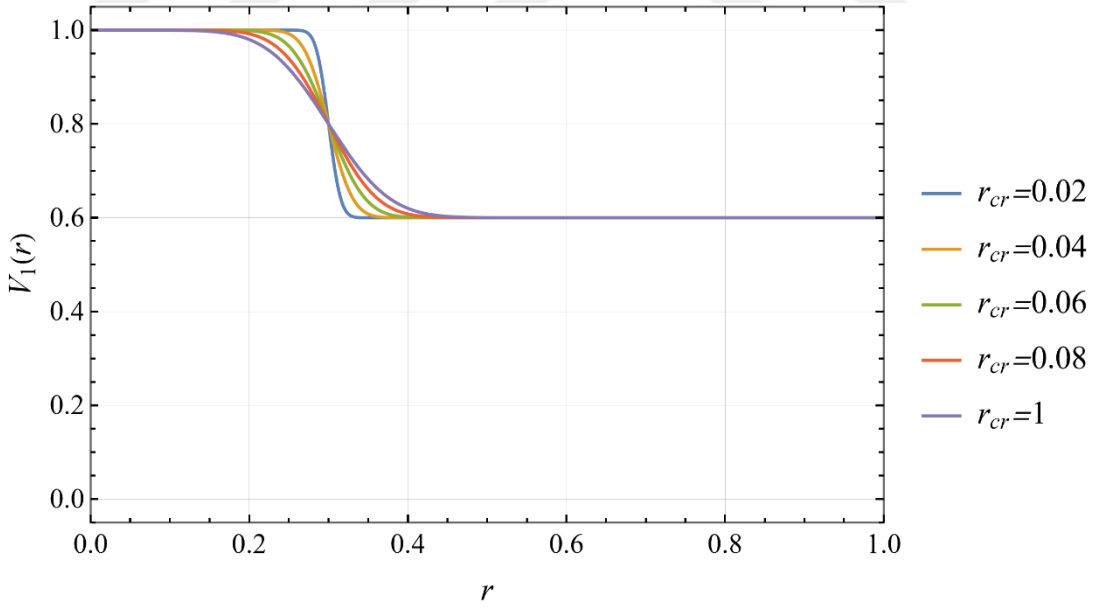

Figure 3.11: Variation of $V_1(r)$ for $r_{cr} = 0.02, 0.04, 0.06, 0.08,$ and 0.1, $r_{ip} = 0.3$, $s_1 = 0.8$, $s_2 = -0.2$ and $p_{cr} = 0.9$

In the next example, we present the case where $V_1(a) = 0.4$, $V_1(b) = 0.9$ and $r_{ip} = 0.3$. From Eq. (3.13) we have $s_1 = 0.65$ and $s_2 = 0.25$. The p_{cr} value and r_{cr} values are selected to be the same as in the previous examples.

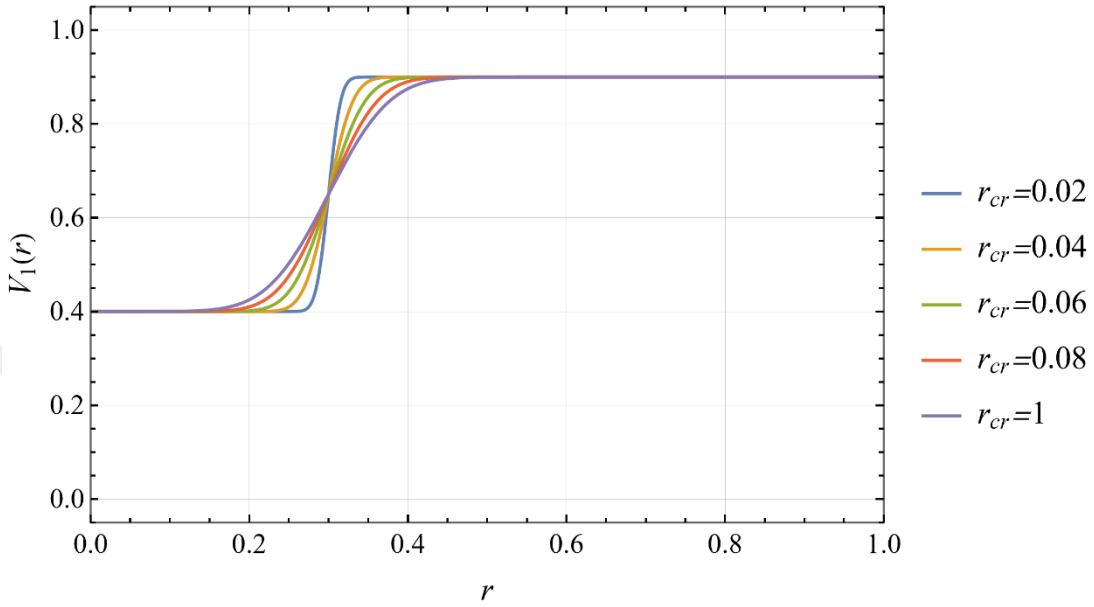

Figure 3.12: Variation of $V_1(r)$ for $r_{cr} = 0.02, 0.04, 0.06, 0.08,$ and 0.1, $r_{ip} = 0.3$, $s_1 = 0.65$, $s_2 = 0.25$ and $p_{cr} = 0.9$

The next two examples show the effects of p_{cr} and r_{ip} on the behavior of $V_1(r)$. Figure 3.13 shows the three different variations of $V_1(r)$ for three different p_{cr} values, that is, for $p_{cr} = 0.3, 0.6,$ and 0.9. In these variations, $V_1(a) = 0.4$, $V_1(b) = 0.9$ and $r_{ip} = 0.3$. From Eq. (3.13) we have $s_1 = 0.65$ and $s_2 = 0.25$. The m values are computed from Eq. (3.11) by preselecting $r_{cr} = 0.02$ as $m = 13.6231, 29.7558,$ and 58.1544. As seen from the figure, $V_1(r)$ changes from 0 to 1 as r increases. $V_1(r)$ has an inflection point at $r_{ip} = 0.3$ and as p_{cr} increases the gradient of variation increases.

By only changing the value of r_{ip} and setting it to $r_{ip} = 0.5$ and taking all the remaining parameters the same as in the previous example, the plot in Fig 3.14 is obtained.

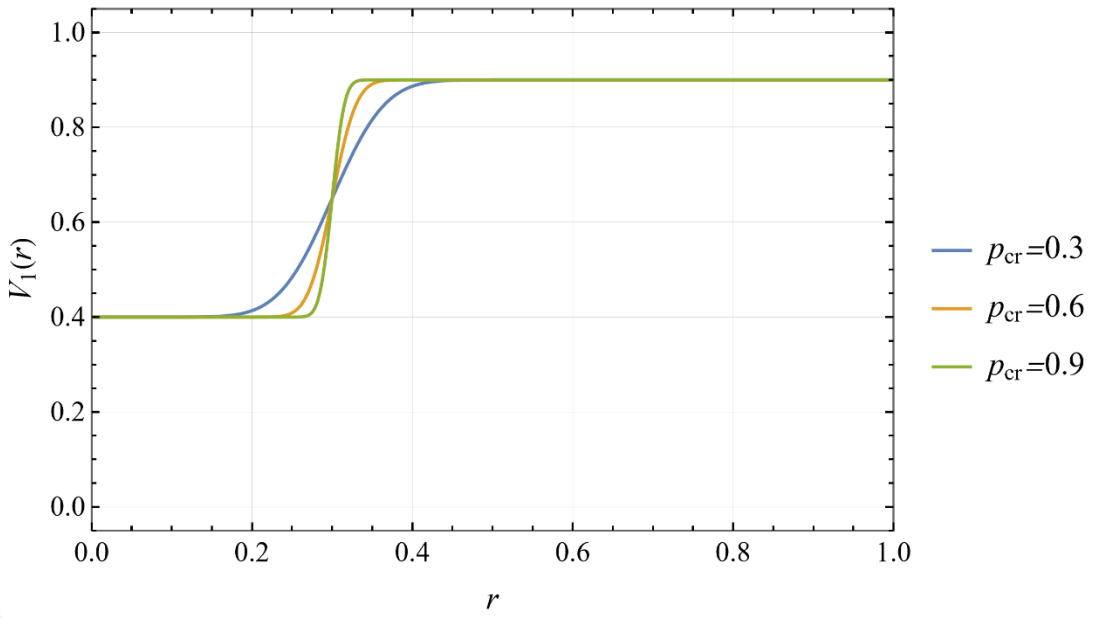

Figure 3.13: Variation of $V_1(r)$ for $s_1 = 0.65,\ s_2 = 0.25, r_{ip} = 0.3, r_{cr} = 0.02$, and $p_{cr} = 0.3, 0.6$, and 0.9

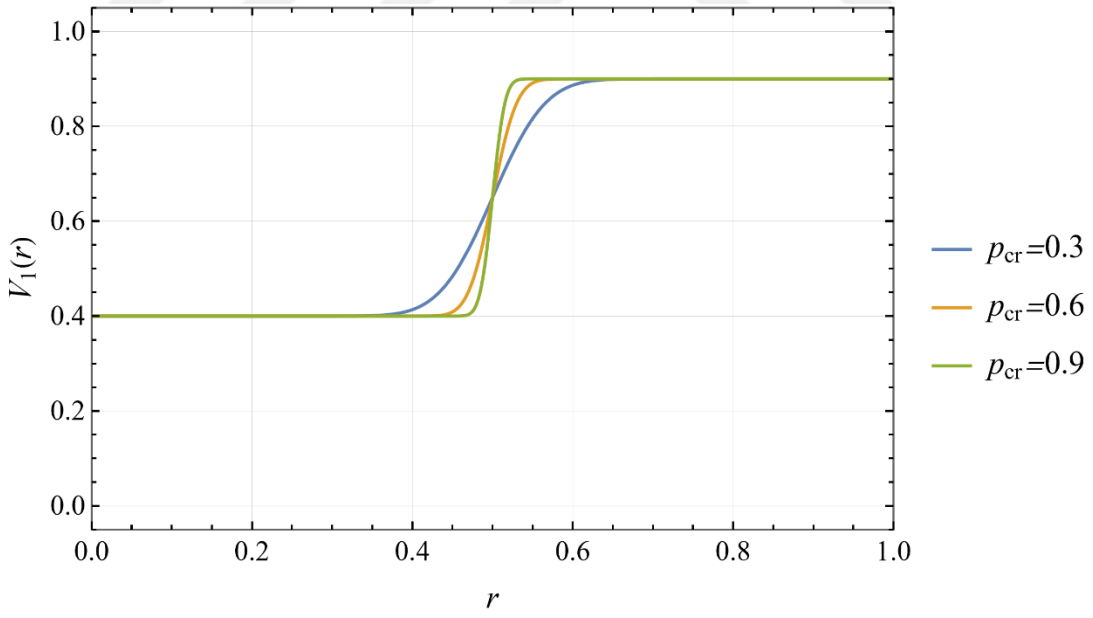

Figure 3.14: Variation of $V_1(r)$ for $s_1 = 0.65,\ s_2 = 0.25, r_{ip} = 0.5, r_{cr} = 0.02$, and $p_{cr} = 0.3, 0.6$, and 0.9

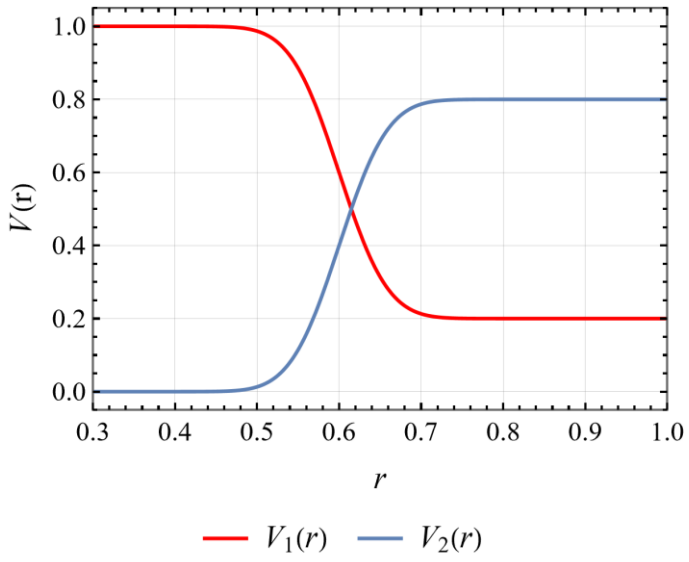

$a = 0.30$	$b = 1.00$
$V_1(a) = 1.00$	$V_1(b) = 0.20$
$s_1 = 0.60$	$s_2 = -0.40$
$V_2(a) = 0.00$	$V_2(b) = 0.80$
$r_{ip} = 0.60$	$r_{cr} = 0.06$
$p_{cr} = 0.80$	$m = 15.1032$

Figure 3.15: Variation of $V_1(r)$ and $V_2(r)$ for the first parameter set

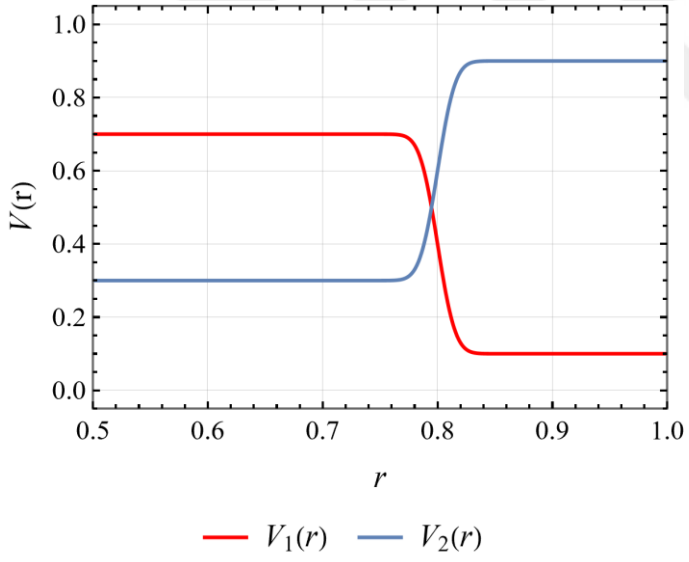

$a = 0.50$	$b = 1.00$
$V_1(a) = 0.70$	$V_1(b) = 0.10$
$s_1 = 0.40$	$s_2 = -0.30$
$V_2(a) = 0.30$	$V_2(b) = 0.90$
$r_{ip} = 0.80$	$r_{cr} = 0.02$
$p_{cr} = 0.90$	$m = 58.1544$

Figure 3.16: Variation of $V_1(r)$and $V_2(r)$ for the second parameter set

The last two figures, Figs 3.15 and 3.16, show the variations of $V_1(r)$ and $V_2(r)$ for different parameter sets on the same graphs. The red and blue lines denote the variations of $V_1(r)$ and $V_2(r)$, respectively. After specifiying the variation of $V_1(r)$, we may easily obtain the variations of $V_2(r)$ from Eq. (3.3).

3.2 Temperature Dependency

In this study, the constituents that form the FGM are taken as Nickel alloy "Inconel 718" and Titanium Alloy "Ti-6Al-4V (Grade 5)". Inconel 718 is a nickel-based super alloy frequently used in nuclear purposes and aircraft engine where components are subjected to high mechanical stresses [74]. For the manufacturing of FGMs containing Inconel 718 we refer to [74-77].

Titanium Alloy (Ti-6Al-4V (Grade 5)) has found widespread use in various industries since its invention in 1954, due to its advantageous strength-to-weight ratio, corrosion resistance and biocompatibility. Common applications include the aerospace, biomedical and high-performance sports industries [78]. For the manufacturing of FGMs containing Titanium Alloy (Ti-6Al-4V (Grade 5)) we refer to [53,78,79].

Combining Ti-6Al-4V with Inconel 718 may be of great importance for aerospace, spacecraft, and other industrial manufacturing applications due to the high strength-to-weight ratio and excellent heat and corrosion resistance properties of the resulting material [80-84].

The variations of physical properties with temperature for these two alloys are obtained from Material Property Database [85]. For all the physical properties, the data is first obtained from the Material Property Database between 300 K and 800 K temperatures with the increments of 10 K. Next, a polynomial is fitted to the corresponding data such that at each point a minimum error tolerance is satisfied. The polynomial fits are expressed in the general form of

$$P(T) = P_{max}\,(c_0 + c_1 T^1 + c_2 T^2 + c_3 T^3 \ldots + c_n T^n) \tag{3.14}$$

In Eq. (3.14), $P = P(T)$ represents the property that is to be considered, which is a function of temperature T in terms of Kelvin's, P_{max} is the maximum value of the material property within the range of that the curve fitting is performed, $c_0, c_1, c_2, c_3, \ldots, c_n$ are the coefficients of the n^{th} degree polynomial.

The polynomial fits are accomplished by using Mathematica's "Fit" function. After importing the data set to Mathematica from the Material Property Database, it is first normalized by dividing all the data values by P_{max}. The polynomial fit is obtained using the normalized data and the degree of the polynomial is arranged such that at each data point the fitted value has an absolute error smaller than 10^{-5}. Table 3.1 and 3.2 depict the parameters of the polynomials that describe the temperature variation of material properties for Inconel 718 and Ti-6Al-4V, respectively.

Figures 3.17 and 3.18 show the comparison of normalized polynomial results with normalized values obtained from the Material Property Database [85]. In these figures, the red dots and blue solid lines represent the data obtained from the Material Property Database and the fitted polynomial, respectively.

Table 3.1: Physical properties of metal nickel chromium alloy (Inconel 718)

Property			P_{max}	c_0	c_1	c_2	c_3	c_4	c_5
Thermal conductivity	k	[W/mK]	1.960738×10^{1}	1.779816×10^{-1}	1.365947×10^{-3}	-5.775842×10^{-7}	1.931858×10^{-10}	-	-
Thermal expansion coefficient	α	[1/K]	1.615100×10^{-5}	1.273838×10^{-1}	3.674703×10^{-3}	-6.105392×10^{-6}	3.594345×10^{-9}	-	-
Modulus of elasticity	E	[GPa]	2.016019×10^{2}	1.048352×10^{0}	-1.415397×10^{-4}	-3.885559×10^{-8}	$-8.862349 \times 10^{-11}$	-	-
Poisson's ratio	ν	[−]	3.012788×10^{-1}	9.367134×10^{-1}	1.275714×10^{-4}	-1.414065×10^{-7}	2.140155×10^{-11}	9.954117×10^{-14}	-
Uniaxial yield limit	σ_U	[MPa]	1.362154×10^{3}	1.286670×10^{0}	-2.039517×10^{-3}	5.474772×10^{-6}	-7.210629×10^{-9}	3.350942×10^{-12}	-
Density	ρ	[g/cm^3]	8.226323×10^{0}	1.007615×10^{0}	-6.744845×10^{-6}	-8.740420×10^{-8}	9.694379×10^{-11}	$-4.227906 \times 10^{-14}$	-

Table 3.2: Physical properties of metal titanium alloy (Ti-6Al-4V (Grade 5))

Property			P_{max}	c_0	c_1	c_2	c_3	c_4	c_5
Thermal conductivity	k	[W/mK]	1.303559×10^{1}	3.105242×10^{-1}	7.211631×10^{-4}	1.758524×10^{-7}	-	-	-
Thermal expansion coefficient	α	[1/K]	1.076555×10^{-5}	5.354354×10^{-1}	9.305391×10^{-4}	-4.372914×10^{-7}	-	-	-
Modulus of elasticity	E	[GPa]	1.048506×10^{2}	1.142117×10^{0}	-4.737269×10^{-4}	-	-	-	-
Poisson's ratio	ν	[−]	3.722886×10^{-1}	8.639604×10^{-1}	1.700495×10^{-4}	-	-	-	-
Uniaxial yield limit	σ_U	[MPa]	8.991059×10^{2}	-1.140588×10^{0}	2.689174×10^{-2}	-1.189510×10^{-4}	2.357930×10^{-7}	$-2.191807 \times 10^{-10}$	7.720676×10^{-14}
Density	ρ	[g/cm^3]	4.469221×10^{0}	1.006460×10^{0}	-1.757771×10^{-5}	-1.464412×10^{-8}	4.860192×10^{-12}	-	-

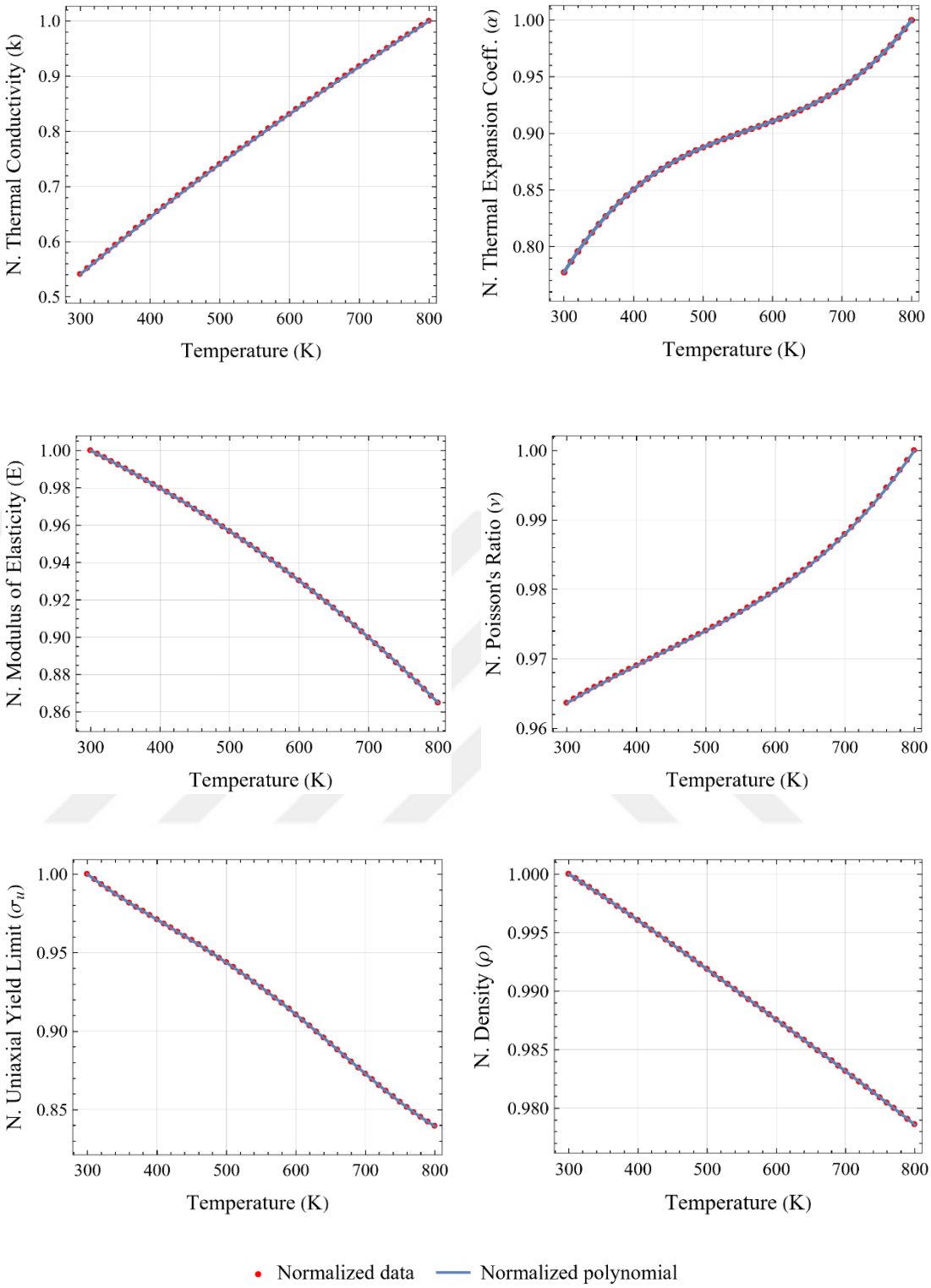

Figure 3.17: Normalized data and normalized polynomials for Inconel 718

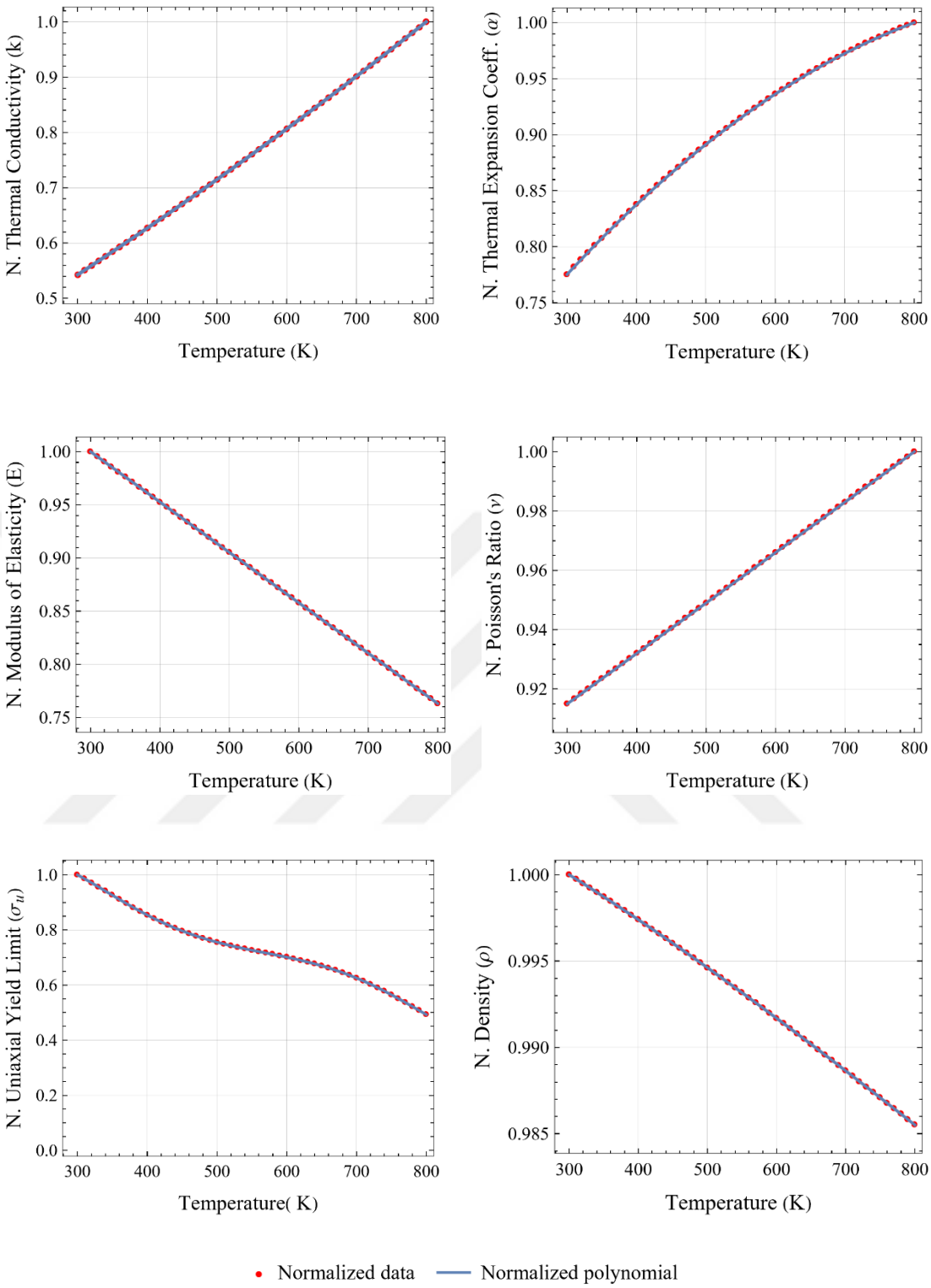

Figure 3.18: Normalized data and normalized polynomials for Ti-6Al-4V (Grade 5)

3.3 FGM Properties with Position-Temperature Dependent Models

In literature there are several methods for describing the effective physical properties of FGMs such as the Voigt method and Mori Tanaka method [68]. In this study, the Voigt method, that is, the rule of mixtures, is used. In the rule of mixtures, an effective physical property P_f is determined from the physical properties P_j and volumetric fractions of V_j of the constituents by using [39,40]

$$P_f = \sum_{j=1}^{n} P_j V_j \tag{3.15}$$

Here n is the number of different constituents that form the FGM and $j = 1 - n$.

In our problem, the number of constituents is two $(n = 2)$, the physical property P_j of the constituents are temperature dependent and V_j is a function of radial coordinate r. Therefore, Eq. (3.15) can be written in the form

$$P_f\,(r,T) = P_1(T)V_1(r) + P_2(T)V_2(r) \tag{3.16}$$

In the above equation $V_2(r)$ can be eliminated by making use of Eq. (3.3) from which we have $V_2(r) = 1 - V_1(r)$. This yields

$$P_f\,(r,T) = P_2(T) + [P_1(T) - P_2(T)]V_1(r) \tag{3.17}$$

which is an alternative form of Eq. (3.16).

The effective physical properties of FGM, thermal conductivity, coefficient of thermal expansion, modulus of elasticity, Poisson's ratio, uniaxial yield limit, and density in our problem can be obtained using Eq. (3.17) as follows:

(a) Thermal conductivity:

$$k_f(r,T) = k_2(T) + [k_1(T) - k_2(T)]V_1(r) \tag{3.18}$$

(b) Coefficient of thermal expansion:

$$\alpha_f(r,T) = \alpha_2(T) + [\alpha_1(T) - \alpha_2(T)]V_1(r) \tag{3.19}$$

(c) Modulus of elasticity:

$$E_f(r,T) = E_2(T) + [E_1(T) - E_2(T)]V_1(r) \tag{3.20}$$

(d) Poisson's ratio:

$$\nu_f(r,T) = \nu_2(T) + [\nu_1(T) - \nu_2(T)]V_1(r) \tag{3.21}$$

(e) Uniaxial yield limit:

$$\sigma_{Uf}(r,T) = \sigma_{U_2}(T) + \left[\sigma_{U_1}(T) - \sigma_{U_2}(T)\right]V_1(r) \tag{3.22}$$

(f) Density:

$$\rho_f(r,T) = \rho_2(T) + \left[\rho_1(T) - \rho_2(T)\right]V_1(r) \tag{3.23}$$

At this point, we present an example with the aim of showing the variations of effective properties of an FGM with radial coordinate and temperature within a tube. The first and second constituents are assumed to be Inconel 718 and Ti-6Al-4V, respectively. The inner and outer radii of the tube are assumed to be $a = 0.3$ and $b = 1.0$, respectively. The following parameters are selected for the error function variation: $V_1(a) = 1.0, V_1(b) = 0.0$ (which gives $s_1 = 0.5$ and $s_2 = 0.5$ from Eq (3.13)), $r_{ip} = 0.5$, $r_{cr} = 0.08$ and $p_{cr} = 0.8$.

The variations of thermal conductivity, thermal expansion coefficient, modulus of elasticity, Poisson's ratio, uniaxial yield limit and density with radial coordinate and temperature are plotted, in the same order through Figs 3.19-3.24. In each figure, the first, second and third columns contain the plots obtained for Inconel 718, Ti-6Al-4V and effective property for the FGM, respectively.

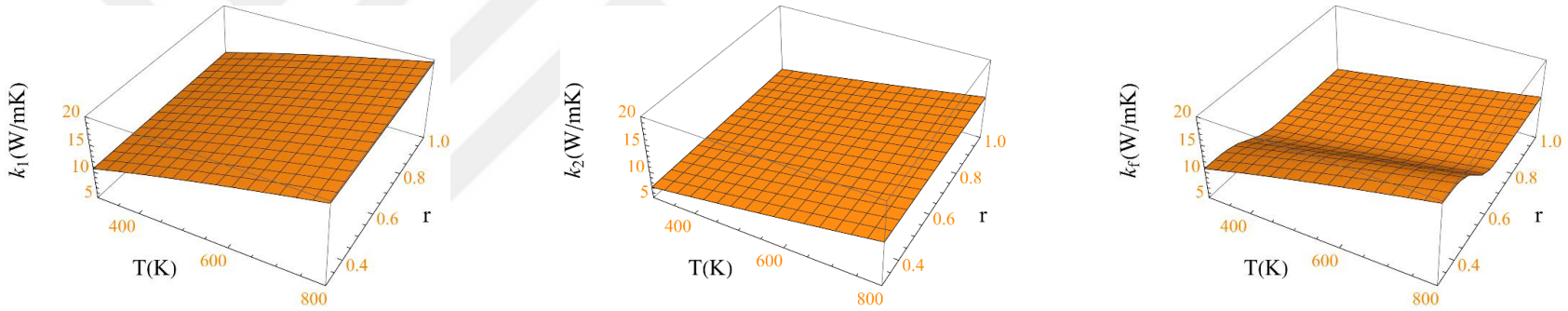

(a) (b) (c)

Figure 3.19: Variations of thermal conductivity (k) with radial coordinate r and temperature. (a) Inconel 718, (b) Ti-6Al-4V (Grade 5), (c) effective thermal conductivity for the FGM

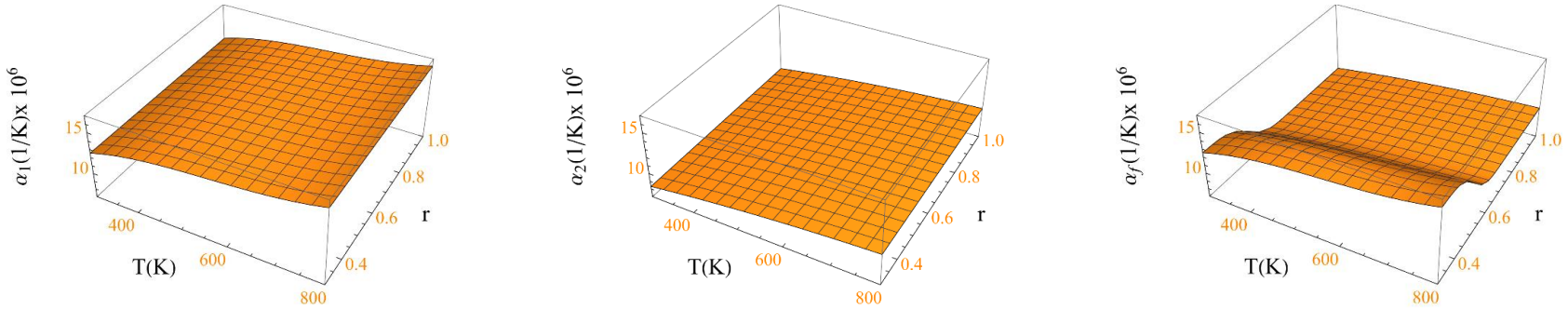

(a) (b) (c)

Figure 3.20: Variations of thermal expansion coefficient (α) with radial coordinate r and temperature. (a) Inconel 718, (b) Ti-6Al-4V (Grade 5), (c) effective thermal expansion coefficient for the FGM

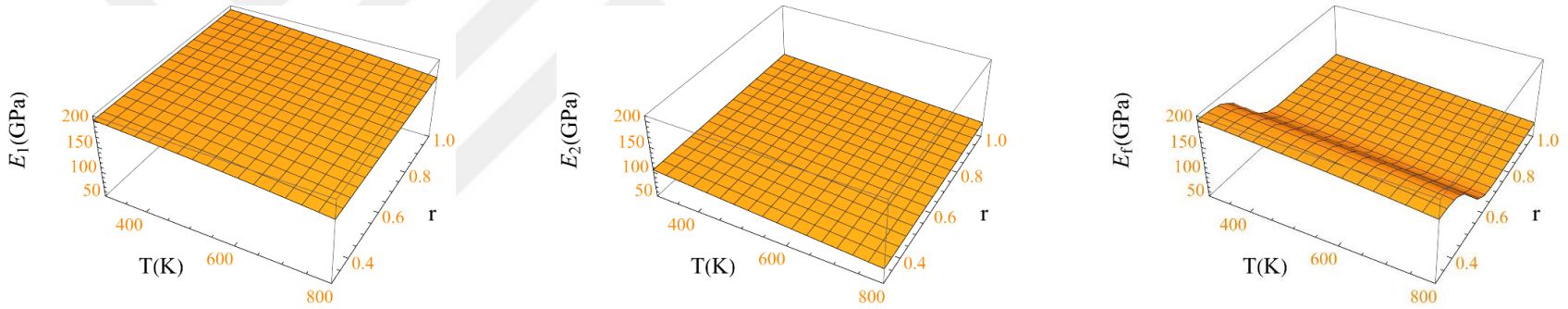

(a) (b) (c)

Figure 3.21: Variations of modulus of elasticity (E) with radial coordinate r and temperature. (a) Inconel 718, (b) Ti-6Al-4V (Grade 5), (c) effective modulus of elasticity for the FGM

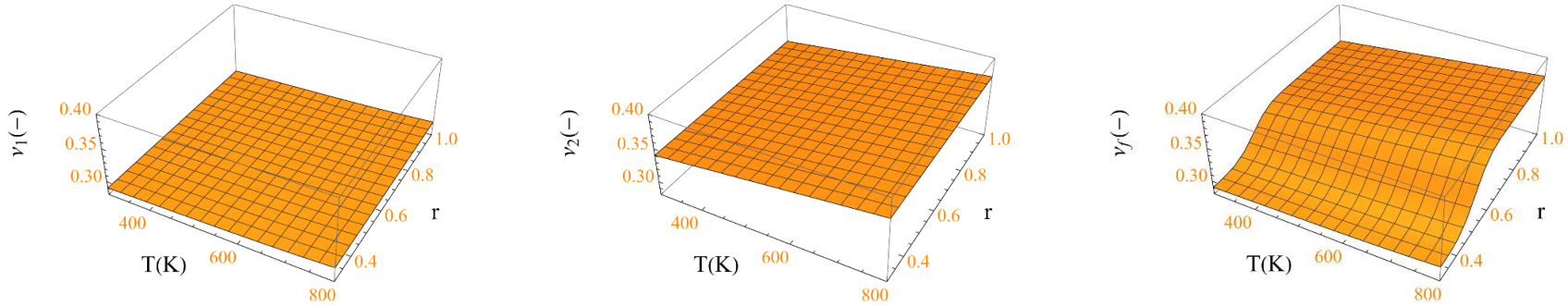

(a) (b) (c)

Figure 3.22: Variations of Poisson's ratio (ν) with radial coordinate r and temperature. (a) Inconel 718, (b) Ti-6Al-4V (Grade 5), (c) effective Poisson's ratio for the FGM

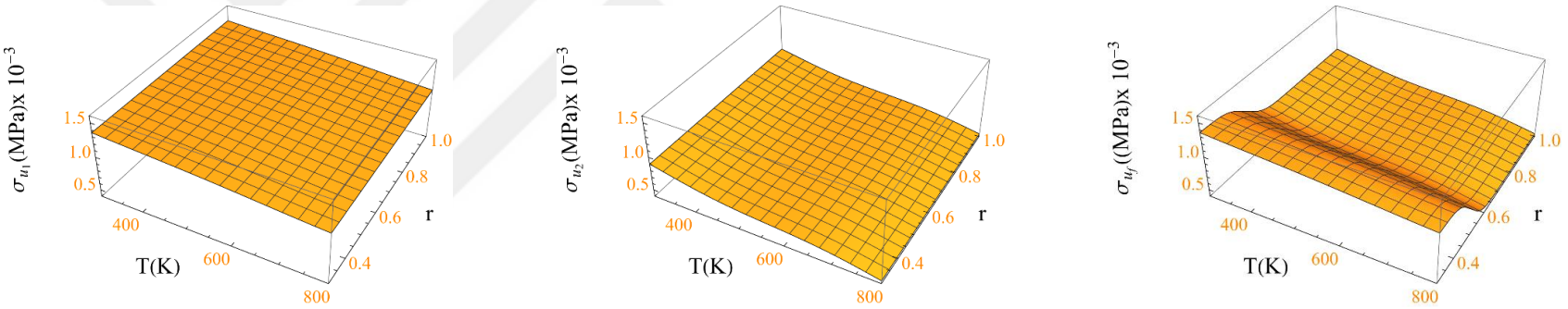

(a) (b) (c)

Figure 3.23: Variations of uniaxial yield limit (σ_U) with radial coordinate r and temperature. (a) Inconel 718, (b) Ti-6Al-4V (Grade 5), (c) effective uniaxial yield limit for the FGM

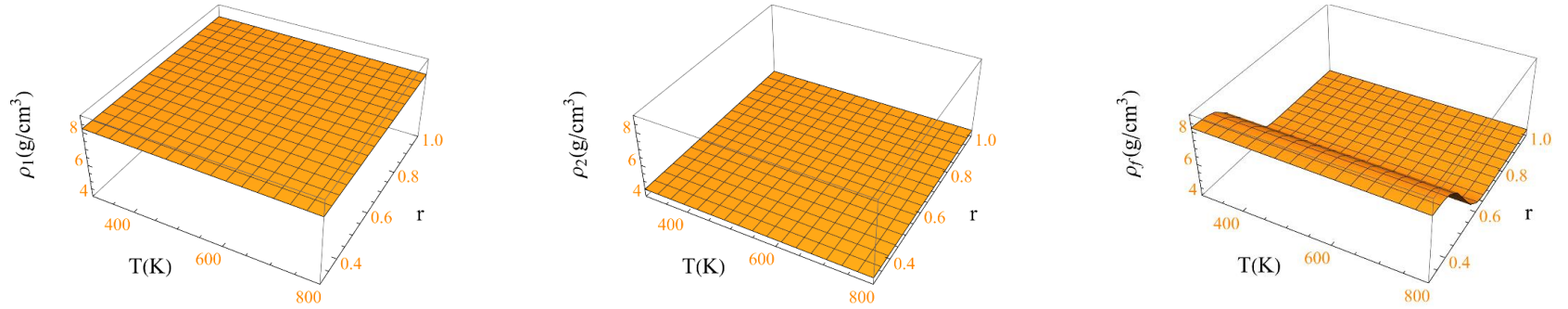

(a) (b) (c)

Figure 3.24: Variations of density (ρ) with radial coordinate r and temperature. (a) Inconel 718, (b) Ti-6Al-4V (Grade 5), (c) effective density for the FGM

CHAPTER 4

SAMPLE PROBLEMS

In this chapter, two sample FGM tube problems are presented. The tubes are assumed to be made of an FGM having two constituents, Inconel 718 and Ti-6Al-4V (Grade 5), where the effective physical properties are determined by the mixture rule presented in Chapter 3.

The differential equations that govern the thermal and mechanical problems (Eqs. (2.3) and (2.21) are solved numerically via Mathematica. We recall that the thermoelastic problem is uncoupled. Therefore, we first obtain the solution for the thermal problem from which we determine the distributions of temperature and its derivative along the radial coordinate of the tube. Then, we solve the mechanical problem and determine the stress components and radial displacement. We also note that the numerical solutions of the thermal problem are obtained using dimensional variables. On the other hand, normalized and nondimensional variables are used for obtaining the solutions and presenting the results of the mechanical problem.

We recall that FGM material is thermoelastic and therefore our solutions are valid in the elastic range. This means that the yielding should not occur for the given thermal and mechanical loads. In the study, it assumed that the FGM material yields according to von Mises yield criterion [86].

Before presenting the sample problems, two important issues should be mentioned. First, the definitions of nondimensional and normalized variables that are used in the solution of mechanical problems are introduced in Section 4.1. Second, von Mises yield criterion and its nondimensional form is presented in Section 4.2. Following these, the first and second sample problems and their solutions are presented in Sections 4.3 and 4.4.

4.1 Nondimensional and normalized quantities

For the presentation of the results pertaining to the elastic deformations of FGM tubes, the following formal variables are used:

- Nondimensional radial coordinate: $\bar{r} = r/b$
- Nondimensional elasticity modulus: $\bar{E} = E/E_R$
- Nondimensional stress components: $\bar{\sigma}_j = \sigma_j/\sigma_{UR}$ where $j = r, \theta, z$
- Normalized strain components: $\bar{\varepsilon}_j = \varepsilon_j E_R/\sigma_{UR}$ where $j = r, \theta$
- Nondimensional radial displacement: $\bar{u} = uE_R/b\ \sigma_{UR}$
- Normalized coefficient of thermal expansion: $\bar{\alpha} = \alpha E_R/\sigma_{UR}$
- Nondimensional heat load: $\bar{Q} = Q\alpha_R\ E_R\ b^2/\sigma_{UR}k_R$

In these definitions, $E_R = E_1(T_0)$, $\sigma_{UR} = \sigma_{U_1}(T_0)$, $\alpha_R = \alpha_1(T_0)$ and $k_R = k_1(T_0)$ are the reference values of elasticity modulus, uniaxial yield limit, coefficient of thermal expansion and thermal conductivity, respectively. T_0 is the reference temperature which is chosen as 300 K in the sample problems that will are presented. The subscript "1" under E_1 , σ_{U_1} , α_1 and k_1 represents that the physical property belongs to the first constituent which is chosen to be Inconel 718 in this study.

4.2 von Mises yield criterion

The condition for the yielding to get started is when the yield stress σ_Y equals to uniaxial yield stress σ_U. This is stated as

$$\sigma_Y = \sigma_U \tag{4.1}$$

according to von Mises yield criterion

$$\sigma_Y = \sqrt{\frac{1}{2}[(\sigma_r - \sigma_\theta)^2 + (\sigma_r - \sigma_z)^2 + (\sigma_\theta - \sigma_z)^2]} \tag{4.2}$$

Substitution of Eq. (4.2) into Eq. (4.1) and dividing the resulting expression by σ_{UR} yields

$$\frac{\sigma_U}{\sigma_{UR}} = \frac{1}{\sigma_{UR}} \sqrt{\frac{1}{2}[(\sigma_r - \sigma_\theta)^2 + (\sigma_r - \sigma_z)^2 + (\sigma_\theta - \sigma_z)^2]} \tag{4.3}$$

which can be rearranged to become

$$1 = \frac{1}{\bar{\sigma}_U} \sqrt{\frac{1}{2}[(\overline{\sigma}_r - \overline{\sigma}_\theta)^2 + (\overline{\sigma}_r - \overline{\sigma}_z)^2 + (\overline{\sigma}_\theta - \overline{\sigma}_z)^2]} \tag{4.4}$$

Equation (4.4) is the yielding condition in terms of nondimensional stress components. During our computations we define a nondimensional stress variable as,

$$\Phi_Y = \frac{1}{\bar{\sigma}_U} \sqrt{\frac{1}{2}[(\overline{\sigma}_r - \overline{\sigma}_\theta)^2 + (\overline{\sigma}_r - \overline{\sigma}_z)^2 + (\overline{\sigma}_\theta - \overline{\sigma}_z)^2]} \tag{4.5}$$

and determine the radial distribution of it. To ensure that the tube remains in the elastic range, the condition $\Phi_Y \leq 1$ is checked. Note that, the radial coordinate at which $\Phi_Y = 1$ is the location where yielding commences.

In our sample problems, the stress response of the tubes made of FGM are also compared with the ones obtained by those made with constituents 1 and 2. In the following discussions the abbreviations "CS_1" and "CS_2" denote, respectively, the tubes made of constituent 1 (Inconel 718) and the tubes made of constituent 2 (Ti-6Al-4V).

In what follows, we drop the bars over the nondimensional and normalized variables/parameters $\bar{a}, \bar{b}, \bar{r}, \bar{E}, \bar{\sigma}_j$ $(j = r, \theta, z)$, $\bar{\varepsilon}_j$ $(j = r, \theta)$, $\bar{u}$ and $\bar{Q}$ for convenience. The temperature and the density are being used in their dimensional forms.

4.3 Sample Problem 1: An FGM tube subjected to internal pressure and prescribed temperatures at the inner at outer surfaces

The cross-section of the tube considered in this problem is shown in the inner and outer radii of the tube are $a = 0.4$ and $b = 1.0$, respectively. The tube is subjected to an internal pressure P and its outer surface is free of stresses. There is no internal heat generation $(Q = 0)$ but the temperature at the inner and outer surfaces are set to $T(0.4) = 800$ K and $T(1.0) = 500$ K, respectively.

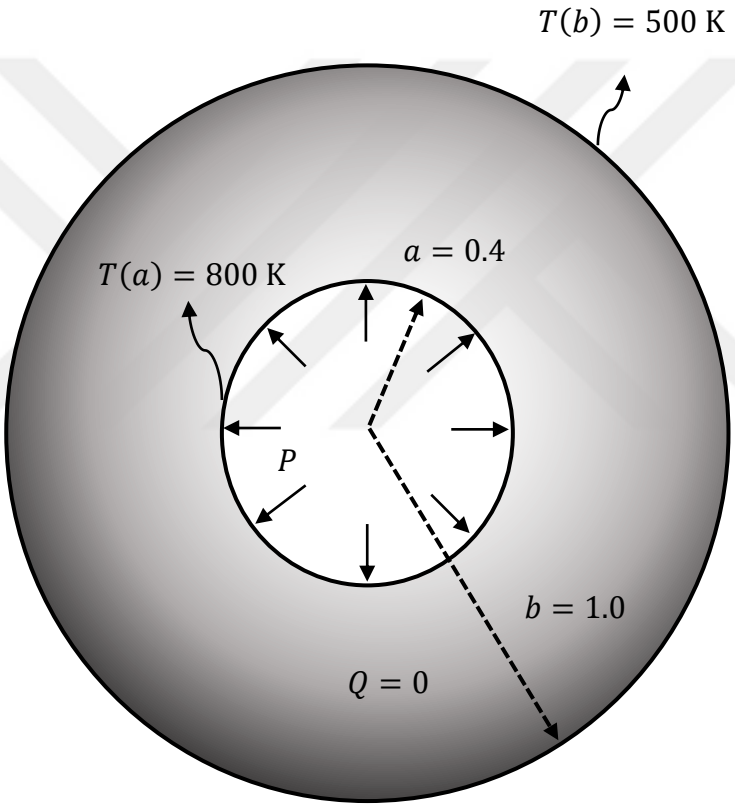

Figure 4.1: The cross-section of the tube considered in Sample Problem 1

Our aim is to determine the maximum value of internal pressure that causes yielding, which is P_Y. As stated above, the solutions for this problem are obtained for three different cases listed below:

(a) Tube made of CS_1 which states the volumetric fraction of constituents are $V_1 = 1$ and $V_2 = 0$.
(b) Tube made of CS_2 which states that $V_1 = 0$ and $V_2 = 1$.
(c) Tube made of FGM with a variation of V_1 based on error function along radial direction given by Eq. (3.12).

Figure 4.2 shows the variation of V_1 along radial direction for Case 3. The error function variation for the FGM tube is defined by setting the parameters as $V_1(a) = 0.3$, $V_1(b) = 1.0$, $p_{cr} = 0.99$, $r_{cr} = 0.05$, and $r_{ip} = 0.6$. From Eq. (3.13) we have $s_1 = 0.65$ and $s_2 = 0.35$.

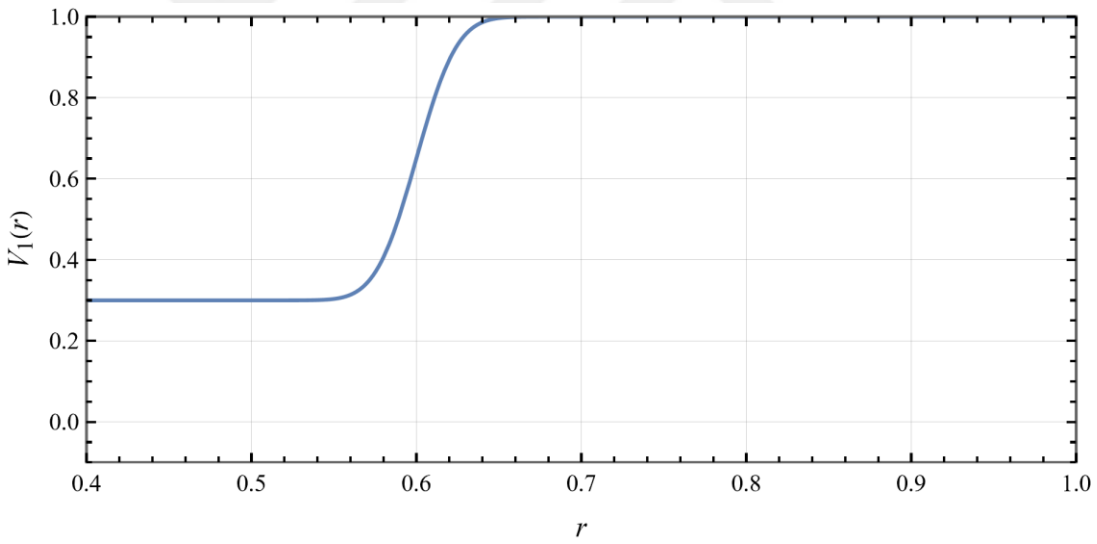

Figure 4.2: The error function variation $V_1(r)$ of the FGM tube for the Sample Problem 1

The nondimensional maximum internal pressure that causes yielding for the three cases are computed as $P_Y^{CS_1} = 0.240679$, $P_Y^{CS_2} = 0.173216$ and $P_Y^{FGM} = 0.269275$. We observe that the FGM tube resists the highest internal pressure without yielding.

The mass per unit length (in which this unit length is also nondimensional), $\widetilde{m}$, of the tube could be calculated from the equation

$$\widetilde{m} = 2\pi \int_a^b \rho(r, T(r)) r \, dr \tag{4.6}$$

Using Eq. (4.6) we compute $\widetilde{m}^{CS_1} = 21417.9$ kg, $\widetilde{m}^{CS_2} = 11687.4$ kg and $\widetilde{m}^{FGM} = 19812.6$ kg. As expected, the first constituent (Inconel 718) has approximately twice mass per unit length of the second constituent (Ti-6Al-4V).

The distributions of temperature and temperature gradient within the tubes are depicted in Figs 4.3a and 4.3b. Table 4.1 shows the values of temperature and temperature gradient at the values of $r = 0.4, 0.5, 0.6, \cdots, 1.0$ ($\Delta r = 0.1$).

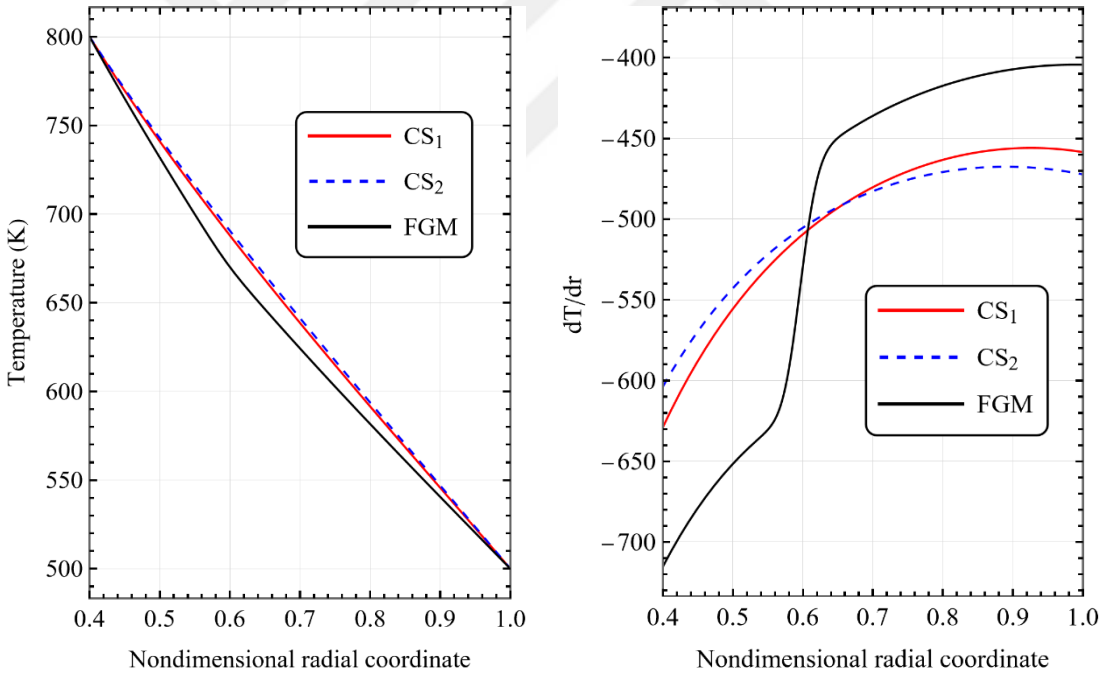

(a) (b)

Figure 4.3: Variations of (a) temperature T and (b) temperature gradient dT/dr with r for the tubes considered in Sample Problem 1

Table 4.1: The values of temperatures and temperature gradients for tubes subjected considered in Sample Problem 1 at $r = 0.4, 0.5, 0.6, \cdots, 1.0$ $(\Delta r = 0.1)$

r	T^{CS_1}	$(dT/dr)^{CS_1}$	T^{CS_2}	$(dT/dr)^{CS_2}$	T^{FGM}	$(dT/dr)^{FGM}$
0.4	8.000000×10^2	-6.289109×10^2	8.000000×10^2	-6.037508×10^2	8.000000×10^2	-7.152586×10^2
0.5	7.410717×10^2	-5.555262×10^2	7.429285×10^2	-5.427445×10^2	7.319637×10^2	-6.515758×10^2
0.6	6.880005×10^2	-5.093557×10^2	6.906767×10^2	-5.052984×10^2	6.701703×10^2	-5.292031×10^2
0.7	6.386381×10^2	-4.802207×10^2	6.413779×10^2	-4.827179×10^2	6.242738×10^2	-4.359834×10^2
0.8	5.915533×10^2	-4.632574×10^2	5.937795×10^2	-4.708125×10^2	5.816830×10^2	-4.173826×10^2
0.9	5.456576×10^2	-4.562188×10^2	5.469278×10^2	-4.675753×10^2	5.405183×10^2	-4.071932×10^2
1.0	5.000000×10^2	-4.585142×10^2	5.000000×10^2	-4.723046×10^2	5.000000×10^2	-4.043688×10^2

From both Fig. 4.3a and Table 4.1, we see that the thermal BC's are satisfied for all the cases, in other words, $T(0.4) = 800$ K and $T(1.0) = 500$ K. It is seen from Fig 4.3a that, the temperature variation for all the cases is close to each other since the temperature at the inner and outer surfaces are prescribed. The results that belong to CS_1 and CS_2 tubes are very close to each other, while the temperature inside the FGM tube is slightly lower than those obtained for the first two cases. This difference becomes more pronounced especially near the inflection point $r_{ip} = 0.6$, also at the region where the slope of dT/dr changes (see Fig. 4.3b).

The variation of stress variable Φ_Y, which is used to check whether the yielding commences or not, with nondimensional radial coordinate is shown in Fig. 4.4. In all cases, the tube starts yielding from the inner surface. This could also be observed from Table 4.2 in which the values of nondimensional stress variable within the tube is given. It should be noted that the elastic limit pressure values for each tube are different when dimensional quantities are used.

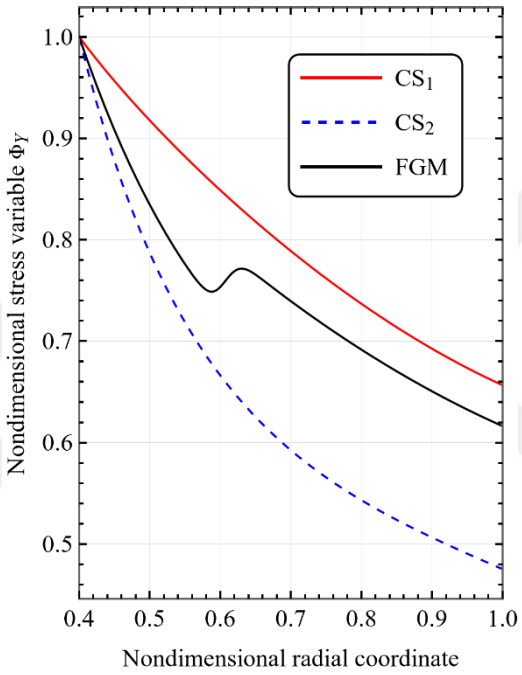

Figure 4.4: Variation of Φ_Y with r for the CS_1, CS_2, and FGM tubes subjected to their corresponding elastic limit pressures considered in Sample Problem 1

Table 4.2: The values of nondimensional stress variables for the CS_1, CS_2, and FGM tubes subjected to their corresponding elastic limit pressures considered in Sample Problem 1 at $r = 0.4, 0.5, 0.6, \cdots, 1.0$ $(\Delta r = 0.1)$

r	$\Phi_Y{}^{CS_1}$	$\Phi_Y{}^{CS_2}$	$\Phi_Y{}^{FGM}$
0.4	9.999998×10^{-1}	1.000005×10^{0}	9.999996×10^{-1}
0.5	9.175658×10^{-1}	7.868450×10^{-1}	8.344244×10^{-1}
0.6	8.487373×10^{-1}	6.661466×10^{-1}	7.535174×10^{-1}
0.7	7.887995×10^{-1}	5.923953×10^{-1}	7.393923×10^{-1}
0.8	7.367468×10^{-1}	5.431736×10^{-1}	6.916076×10^{-1}
0.9	6.925135×10^{-1}	5.064583×10^{-1}	6.505610×10^{-1}
1.0	6.565753×10^{-1}	4.752579×10^{-1}	6.162577×10^{-1}

The variation of stress components for the corresponding elastic limit pressures is shown in Fig. 4.5, whereas the variation strain components and the radial displacement are depicted in Fig. 4.6. Similarly, tabulated values of these variables which are taken into account are given in Tables 4.3 and 4.4.

From Fig. 4.5a and also from the second through fourth columns of Table 4.3, we observe that the mechanical BC's are satisfied for all the cases investigated. At the inner surface of the tubes the radial stress component $\sigma_r(0.4) = -P_Y$,while, at outer surface the radial stress becomes $\sigma_r(1.0) \approx 0$ due to numerical precision (the last row, second through fourth columns of Table 4.3).

In the absolute sense, the stress and strain components for CS_2 tube have smaller values than those determined for CS_1 tube (See Figs 4.5, 4.6 and Tables 4.3 and 4.4) under corresponding elastic limit pressures. When we investigate the distributions of σ_θ , σ_z and ε_r for the FGM tube, it is seen that, the values are closer to those corresponding to CS_2 from the inner surface up to approximately $r = 0.56$. From this point, these values show sudden changes in their slope and make sharp decreases (σ_θ and σ_z) or increase (ε_r) until $r = 0.64$. After this point, the values come closer to those of CS_1.

We recall that, the FGM tube is graded such that from the inner surface to the radial coordinates closer to r_{ip} the second constituent is dominant. On the other hand, as radial coordinate increases, the first constituent becomes dominant (see Fig. 4.2). The effect of material gradation is quite clear in these figures.

When we investigate the variations σ_r, ε_θ and u for the FGM tube, it is observed that, the slopes show slight changes near $r_{ip} = 0.6$. From Fig. 4.6a and Table 4, we see that, the values of radial displacement at the inner surface for CS_1 and CS_2 tubes are almost the same, whereas a higher value for the FGM tube is obtained.

Table 4.3: The values of nondimensional stress components at $r = 0.4, 0.5, 0.6, \cdots, 1.0$ $(\Delta r = 0.1)$ for the CS_1, CS_2, and FGM tubes subjected to their corresponding elastic limit pressures considered in Sample Problem 1

r	${\sigma_r}^{CS_1}$	${\sigma_r}^{CS_2}$	${\sigma_r}^{FGM}$	${\sigma_\theta}^{CS_1}$	${\sigma_\theta}^{CS_2}$	${\sigma_\theta}^{FGM}$	${\sigma_z}^{CS_1}$	${\sigma_z}^{CS_2}$	${\sigma_z}^{FGM}$
0.4	-2.406790×10^{-1}	-1.732176×10^{-1}	-2.692750×10^{-1}	-1.987299×10^{-1}	3.781583×10^{-2}	2.307230×10^{-2}	-1.058532×10^{0}	-3.368295×10^{-1}	-5.304353×10^{-1}
0.5	-2.164224×10^{-1}	-1.290839×10^{-1}	-2.059653×10^{-1}	-4.769192×10^{-2}	5.843416×10^{-2}	7.243109×10^{-2}	-9.056016×10^{-1}	-2.855092×10^{-1}	-4.377543×10^{-1}
0.6	-1.780986×10^{-1}	-9.571244×10^{-2}	-1.555325×10^{-1}	7.114433×10^{-2}	8.441125×10^{-2}	1.057801×10^{-1}	-7.662858×10^{-1}	-2.372216×10^{-1}	-5.228259×10^{-1}
0.7	-1.349961×10^{-1}	-6.797200×10^{-2}	-1.177736×10^{-1}	1.742805×10^{-1}	1.128237×10^{-1}	1.467938×10^{-1}	-6.346877×10^{-1}	-1.906105×10^{-1}	-6.116179×10^{-1}
0.8	-9.032719×10^{-2}	-4.351774×10^{-2}	-7.917481×10^{-2}	2.695518×10^{-1}	1.427139×10^{-1}	2.341909×10^{-1}	-5.070616×10^{-1}	-1.447605×10^{-1}	-4.958532×10^{-1}
0.9	-4.522220×10^{-2}	-2.110721×10^{-2}	-3.972696×10^{-2}	3.613853×10^{-1}	1.738484×10^{-1}	3.170120×10^{-1}	-3.807088×10^{-1}	-9.895761×10^{-2}	-3.824043×10^{-1}
1.0	-3.540143×10^{-9}	4.611588×10^{-9}	-5.633592×10^{-8}	4.527412×10^{-1}	2.063247×10^{-1}	3.979324×10^{-1}	-2.534144×10^{-1}	-5.256628×10^{-2}	-2.694984×10^{-1}

Table 4.4: The values of normalized strain components and nondimensional radial displacements at $r = 0.4, 0.5, 0.6, \cdots, 1.0$ $(\Delta r = 0.1)$ for the CS_1, CS_2, and FGM tubes subjected to their corresponding elastic limit pressures considered in Sample Problem 1

r	${\varepsilon_r}^{CS_1}$	${\varepsilon_r}^{CS_2}$	${\varepsilon_r}^{FGM}$	${\varepsilon_\theta}^{CS_1}$	${\varepsilon_\theta}^{CS_2}$	${\varepsilon_\theta}^{FGM}$	u^{CS_1}	u^{CS_2}	u^{FGM}
0.4	1.230527×10^{0}	5.656947×10^{-1}	6.566714×10^{-1}	1.293643×10^{0}	1.295351×10^{0}	1.391761×10^{0}	5.174572×10^{-1}	5.181405×10^{-1}	5.567042×10^{-1}
0.5	1.010347×10^{0}	5.209658×10^{-1}	5.613049×10^{-1}	1.257708×10^{0}	1.145485×10^{0}	1.235475×10^{0}	6.288542×10^{-1}	5.727423×10^{-1}	6.177375×10^{-1}
0.6	8.443555×10^{-1}	4.558690×10^{-1}	6.542901×10^{-1}	1.202149×10^{0}	1.036134×10^{0}	1.119788×10^{0}	7.212895×10^{-1}	6.216803×10^{-1}	6.718727×10^{-1}
0.7	7.046855×10^{-1}	3.831928×10^{-1}	6.930522×10^{-1}	1.140840×10^{0}	9.480102×10^{-1}	1.064341×10^{0}	7.985880×10^{-1}	6.636714×10^{-1}	7.450390×10^{-1}
0.8	5.786443×10^{-1}	3.073728×10^{-1}	5.767807×10^{-1}	1.078344×10^{0}	8.727712×10^{-1}	1.010552×10^{0}	8.626750×10^{-1}	6.982169×10^{-1}	8.084419×10^{-1}
0.9	4.593847×10^{-1}	2.299099×10^{-1}	4.685313×10^{-1}	1.016156×10^{0}	8.056582×10^{-1}	9.562887×10^{-1}	9.145404×10^{-1}	7.250924×10^{-1}	8.606599×10^{-1}
1.0	3.425841×10^{-1}	1.510961×10^{-1}	3.643276×10^{-1}	9.546327×10^{-1}	7.441545×10^{-1}	9.022818×10^{-1}	9.546327×10^{-1}	7.441545×10^{-1}	9.022818×10^{-1}

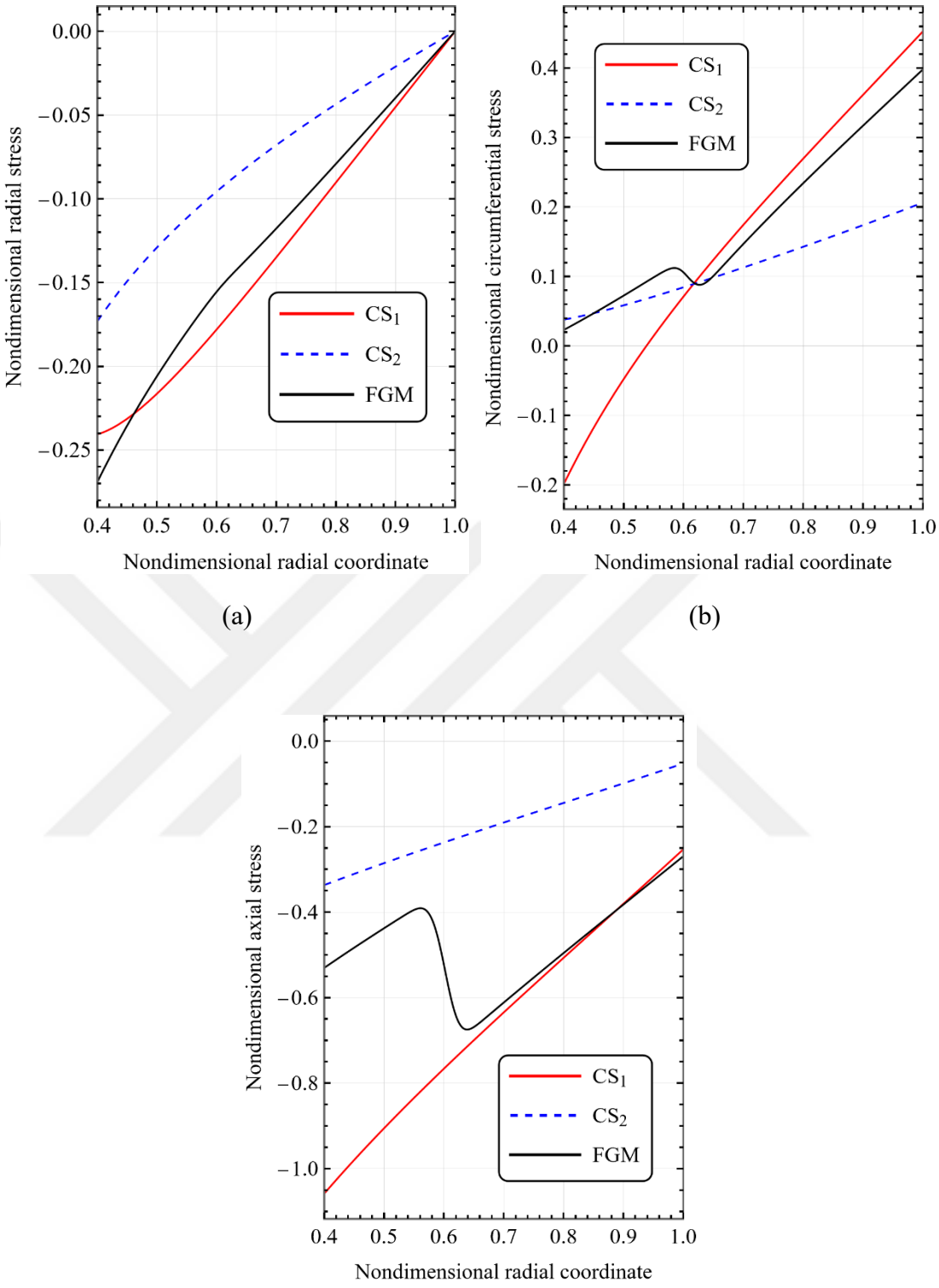

Figure 4.5: Variations of (a) the radial stress σ_r, (b) the circumferential stress σ_θ, and (c) the axial stress σ_z with r for the CS_1, CS_2, and FGM tubes subjected to their corresponding elastic limit pressures considered in Sample Problem 1

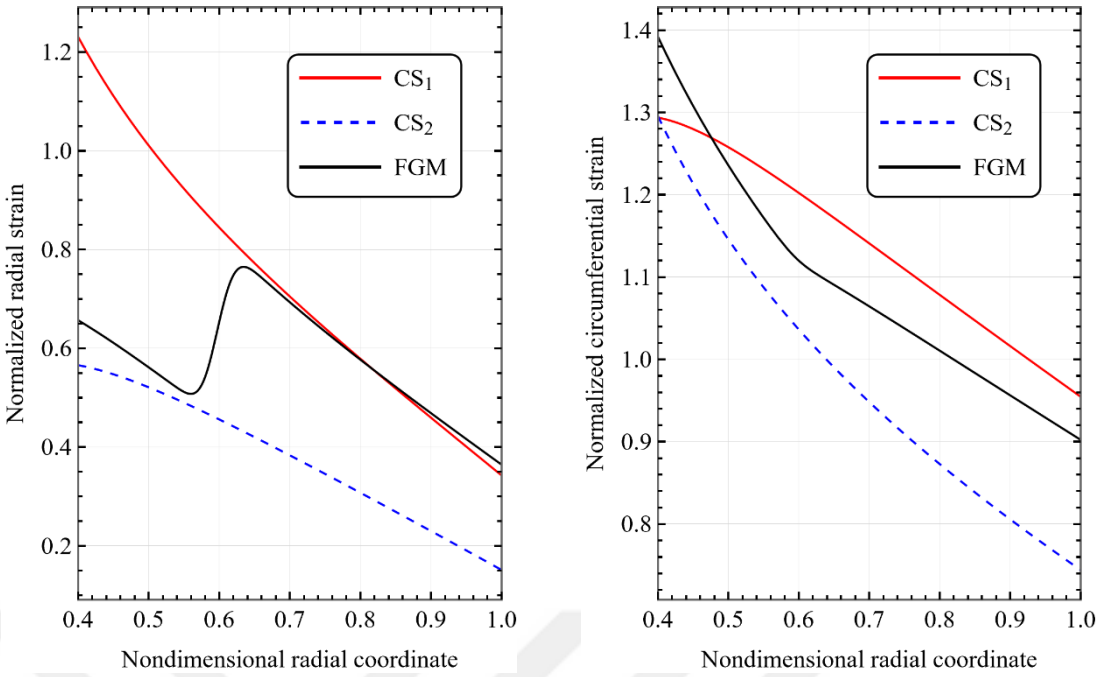

(a)

(b)

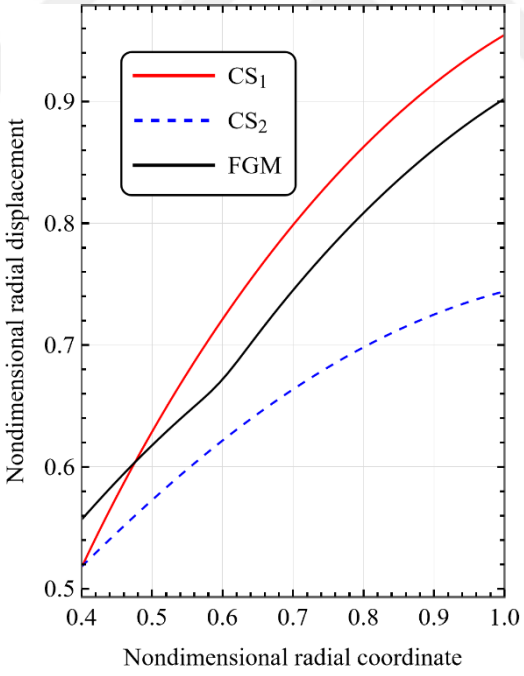

(c)

Figure 4.6: Variations of (a) the radial strain ε_r, (b) the circumferential strain ε_θ, and (c) the radial displacement u with r for the CS_1, CS_2, and FGM tubes subjected to their corresponding elastic limit pressures considered in Sample Problem 1

4.4 Sample Problem 2: An internally heat generating FGM tube having a prescribed temperature at the inner surface and insulated outer surface embedded in a rigid casing

The cross-section of the tube considered in this problem is shown in Figure 4.7. The inner and outer radii of the tube are $a = 0.5$ and $b = 1.0$, respectively. The tube has an internal heat generation Q, the temperature at the inner surface is set to to $T(0.5) = 400$ K while the outer surface is insulated. The inner surface of the tube is free of tractions and the displacement at the outer surface is assumed to be zero, $u(1.0) = 0$.

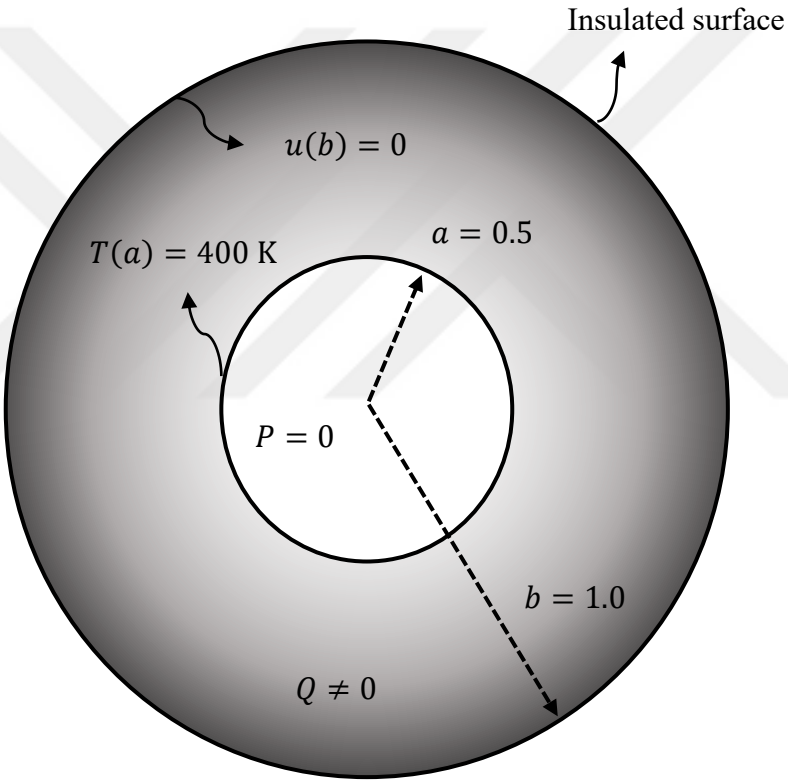

Figure 4.7: The cross-section of the tube considered in Sample Problem 2

The aim of this problem is to determine the maximum value of heat load that causes yielding, that is Q_Y. Similar to the first problem, three different cases are considered. These are tubes made of (a) CS_1, (b) CS_2, and (c) FGM. The variation of V_1 along r in the FGM tube is again based on the error function given by Eq. (3.12).

Figure 4.8 shows the variation of V_1 along radial direction for Case 3. The error function variation for the FGM tube is defined by setting the parameters as $V_1(a) = 1.0, V_1(b) = 0.3, p_{cr} = 0.99$, $r_{cr} = 0.1$, and $r_{ip} = 0.8$. From Eq. (3.13) we have $s_1 = 0.65$ and $s_2 = -0.35$.

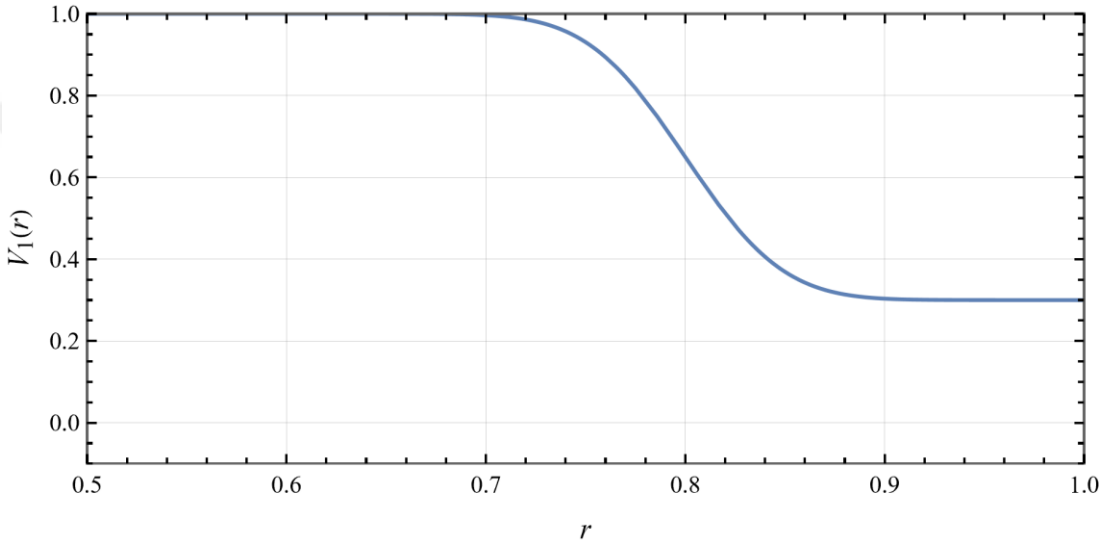

Figure 4.8: The error function variation $V_1(r)$ of the FGM tube for the Sample Problem 2

The nondimensional heat loads that cause yielding for the three cases are computed as $Q_Y^{CS_1} = 3.15290$, $Q_Y^{CS_2} = 3.11418$ and $Q_Y^{FGM} = 3.78979$. We observe that the FGM tube resists the highest heat load without yielding. It should be noted that the elastic limit pressure values for each tube are different when dimensional quantities are used.

The mass per unit length, $\tilde{m}$, of the tube are also calculated using Eq. (4.6). They are obtained as $\tilde{m}^{CS_1} = 19170.9$ kg, $\tilde{m}^{CS_2} = 10426.6$ kg, and $\tilde{m}^{FGM} = 16239.3$ kg.

The variations of temperature and temperature gradient within the tubes are shown in Figs. 4.9a and 4.9b. Table 4.5 shows the values of temperature and temperature gradient values at $r = 0.5, 0.6, \cdots, 1.0$ ($\Delta r = 0.1$). From both Figs. 4.9a, and 4.9b, and Table 4.5, we see that the thermal BC's are satisfied for all the cases.

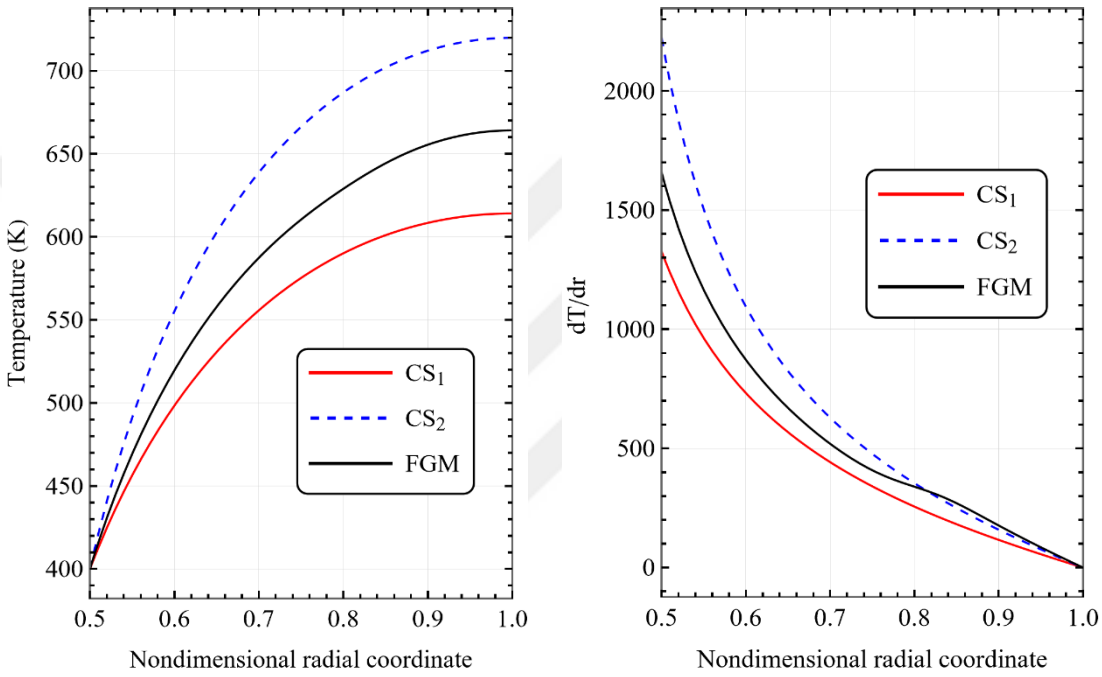

(a) (b)

Figure 4.9: Variations of (a) temperature T and (b) temperature gradient dT/dr with r for the tubes considered in Sample Problem 2

Table 4.5: The values of temperatures and temperature gradients for the tubes considered in Sample Problem 2 at $r = 0.5,0.6,0.7,\cdots,1.0$ $(\Delta r = 0.1)$

r	T^{CS_1}	$(dT/dr)^{CS_1}$	T^{CS_2}	$(dT/dr)^{CS_2}$	T^{FGM}	$(dT/dr)^{FGM}$
0.5	4.000000×10^2	1.325636×10^3	4.000000×10^2	2.222677×10^3	4.000000×10^2	1.657823×10^3
0.6	4.983790×10^2	7.317574×10^2	5.552152×10^2	1.093644×10^3	5.196423×10^2	8.710333×10^2
0.7	5.557814×10^2	4.420378×10^2	6.388186×10^2	6.282063×10^2	5.874298×10^2	5.190257×10^2
0.8	5.901174×10^2	2.555555×10^2	6.869709×10^2	3.537863×10^2	6.289720×10^2	3.391718×10^2
0.9	6.084261×10^2	1.159858×10^2	7.121522×10^2	1.585023×10^2	6.555188×10^2	1.763129×10^2
1.0	6.140900×10^2	3.706927×10^{-6}	7.198773×10^2	2.074303×10^{-5}	6.641167×10^2	3.023594×10^{-5}

The thermal BC's are, $T(0.4) = 400$ K and $[dT/dr]_{r=1} \approx 0$, since the outer surface is insulated. Temperature starts from 400 K at the inner surface (the thermal BC at the inner surface) for all the tubes. CS_1 has the lowest values whereas CS_2 has the highest values within the tube. The temperature variation of the FGM tube is in between CS_1 and CS_2. A similar trend can be seen up to $r_{ip} = 0.8$ when the variation of temperature gradient is analyzed in Fig 4.9b. However, after $r_{ip} = 0.8$, the temperature gradient values of CS_2 and FGM are almost the same up the outer surface.

The variation of stress variable Φ_Y with nondimensional radial coordinate is shown in Fig. 4.10. This could also be observed from Table 4.6 in which the values of nondimensional stress variable within the tube is given.

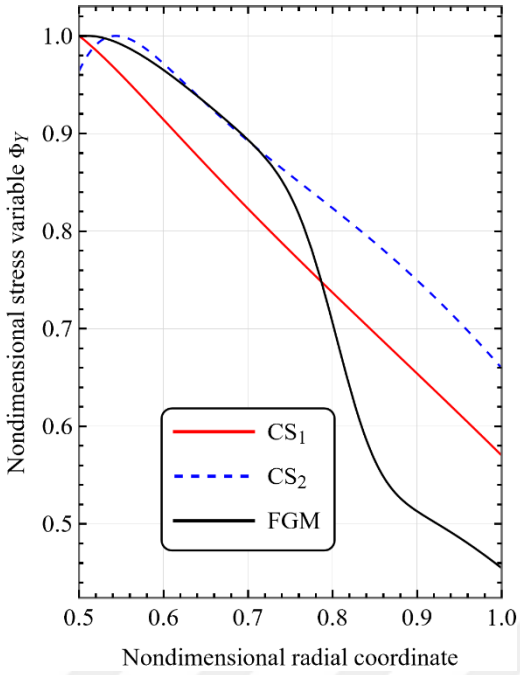

Figure 4.10: Variation of Φ_Y with r for the CS_1, CS_2, and FGM tubes subjected to their corresponding elastic limit heat loads considered in Sample Problem 2

Table 4.6: The values of nondimensional stress variables for the CS_1, CS_2, and FGM tubes subjected to their corresponding elastic limit heat loads considered in Sample Problem 2 at $r = 0.5, 0.6, 0.7, \cdots, 1.0$ $(\Delta r = 0.1)$

r	$\Phi_Y{}^{CS_1}$	$\Phi_Y{}^{CS_2}$	$\Phi_Y{}^{FGM}$
0.5	9.999997×10^{-1}	9.640449×10^{-1}	9.991468×10^{-1}
0.6	9.141154×10^{-1}	9.716022×10^{-1}	9.649865×10^{-1}
0.7	8.228522×10^{-1}	8.923360×10^{-1}	8.934579×10^{-1}
0.8	7.369633×10^{-1}	8.234104×10^{-1}	7.059668×10^{-1}
0.9	6.540573×10^{-1}	7.495799×10^{-1}	5.129427×10^{-1}
1.0	5.702170×10^{-1}	6.596131×10^{-1}	4.547605×10^{-1}

The CS_1 tube starts to yield at the inner surface, whereas the CS_2 and FGM tubes start to yield inside the tube at the radial coordinates $r = 0.5436$ and $r = 0.5104$, respectively. For the values of r smaller than 0.52, Φ_Y values for CS_2 are higher than those of CS_1. On the other hand, Φ_Y variation of FGM tube is closer to CS_2 up to $r = 0.74$ and then it starts to decrease more rapidly than Φ_Y of the other two tubes. Finally, around $r_{ip} = 0.8$ it has the lowest values, and this trend continues up to the outer surface. Table 4.5 shows the values of Φ_Y within the tubes at $r = 0.5, \cdots, 1.0$ ($\Delta r = 0.1$) .

Figures 4.11 and 4.12 depict the variations of stress and strain components and radial displacements of the CS_1, CS_2, and FGM tubes, respectively. Tables 4.7 and 4.8 are presented for the same purpose. From Fig. 4.11a and from the second through fourth columns of Table 4.7, we observe that the mechanical BC at the inner surface of the tubes is satisfied ($\sigma_r(0.5) = 0.0$).

The second mechanical BC, radial displacement being zero at the outer surface, is also satisfied for all types of tubes, which can be identified from Fig. 4.11c and from the last row, eighth through tenth columns of Table 4.7. It is seen from those figures and table that $u(1.0) \approx 0$.

The differences between variations of stress and strain components in this problem are more dominant than those obtained for the previous problem. In the absolute sense, σ_r, σ_θ, and σ_z of CS_2 tube have smaller values than those determined for CS_1 and FGM tubes (See Fig 4.11 and Table 4.7). On the other hand, radial strain ε_θ of CS_2 behaves oppositely.

There is a sudden change in the slopes in between $r = 0.7$ and $r = 0.9$ of the distributions of σ_θ , σ_z, and ε_r for the FGM tube, which is due to the effect of the change in the volumetric content of gradients in the same interval. For the FGM tube, the values of σ_r is very close to σ_r values of CS_1 tube up to the inflection point $r_{ip} = 0.8$, and after this point, the radial stress smoothly separates from the variation of CS_1.

In case we investigate ε_θ and u variations for the FGM tube, it is observed that, they appear to be very close those corresponding to CS_1 tube. We recall that, in this sample problem, the FGM tube is graded such that from the inner surface to the radial coordinates closer to r_{ip} the first constituent is dominant. Whereas as radial coordinate increases the second constituent becomes dominant (see Fig. 4.8).

Table 4.7: The values of nondimensional stress components at $r = 0.5, 0.6, 0.7, \cdots, 1.0$ $(\Delta r = 0.1)$ for the CS_1, CS_2, and FGM tubes subjected to their corresponding elastic limit heat loads considered in Sample Problem 2

r	${\sigma_r}^{CS_1}$	${\sigma_r}^{CS_2}$	${\sigma_r}^{FGM}$	${\sigma_\theta}^{CS_1}$	${\sigma_\theta}^{CS_2}$	${\sigma_\theta}^{FGM}$	${\sigma_z}^{CS_1}$	${\sigma_z}^{CS_2}$	${\sigma_z}^{FGM}$
0.5	0.000000×10^{0}	0.000000×10^{0}	0.000000×10^{0}	-1.120338×10^{0}	-6.265882×10^{-1}	-1.119390×10^{0}	-5.186246×10^{-1}	-2.811252×10^{-1}	-5.183480×10^{-1}
0.6	-1.932026×10^{-1}	-1.059877×10^{-1}	-1.979765×10^{-1}	-1.183271×10^{0}	-6.387241×10^{-1}	-1.232185×10^{0}	-7.870483×10^{-1}	-4.239261×10^{-1}	-8.442169×10^{-1}
0.7	-3.355685×10^{-1}	-1.815703×10^{-1}	-3.480632×10^{-1}	-1.190863×10^{0}	-6.297849×10^{-1}	-1.254977×10^{0}	-9.422561×10^{-1}	-4.992415×10^{-1}	-1.023826×10^{0}
0.8	-4.416464×10^{-1}	-2.366740×10^{-1}	-4.522763×10^{-1}	-1.174551×10^{0}	-6.142572×10^{-1}	-1.018039×10^{0}	-1.034081×10^{0}	-5.418678×10^{-1}	-9.225936×10^{-1}
0.9	-5.214443×10^{-1}	-2.775734×10^{-1}	-4.988160×10^{-1}	-1.142813×10^{0}	-5.946223×10^{-1}	-8.082992×10^{-1}	-1.082746×10^{0}	-5.639748×10^{-1}	-7.781283×10^{-1}
1.0	-5.814387×10^{-1}	-3.081237×10^{-1}	-5.288230×10^{-1}	-1.097777×10^{0}	-5.707603×10^{-1}	-7.882545×10^{-1}	-1.097777×10^{0}	-5.707603×10^{-1}	-7.882546×10^{-1}

Table 4.8: The values of normalized strain components and nondimensional radial displacements at $r = 0.5, 0.6, 0.7, \cdots, 1.0$ $(\Delta r = 0.1)$ for the CS_1, CS_2, and FGM tubes subjected to their corresponding elastic limit heat loads considered in Sample Problem 2

r	${\varepsilon_r}^{CS_1}$	${\varepsilon_r}^{CS_2}$	${\varepsilon_r}^{FGM}$	${\varepsilon_\theta}^{CS_1}$	${\varepsilon_\theta}^{CS_2}$	${\varepsilon_\theta}^{FGM}$	u^{CS_1}	u^{CS_2}	u^{FGM}
0.5	6.838178×10^{-1}	7.642883×10^{-1}	6.834531×10^{-1}	-7.933722×10^{-1}	-9.392019×10^{-1}	-7.924876×10^{-1}	-3.966861×10^{-1}	-4.696010×10^{-1}	-3.962438×10^{-1}
0.6	8.024531×10^{-1}	9.435025×10^{-1}	8.783594×10^{-1}	-5.354087×10^{-1}	-6.374266×10^{-1}	-5.273198×10^{-1}	-3.212452×10^{-1}	-3.824560×10^{-1}	-3.163919×10^{-1}
0.7	8.332207×10^{-1}	9.910352×10^{-1}	9.389610×10^{-1}	-3.414353×10^{-1}	-4.072548×10^{-1}	-3.211803×10^{-1}	-2.390047×10^{-1}	-2.850783×10^{-1}	-2.248262×10^{-1}
0.8	8.222354×10^{-1}	9.808936×10^{-1}	8.238211×10^{-1}	-1.949562×10^{-1}	-2.326598×10^{-1}	-1.671853×10^{-1}	-1.559649×10^{-1}	-1.861278×10^{-1}	-1.337483×10^{-1}
0.9	7.836090×10^{-1}	9.352308×10^{-1}	6.482654×10^{-1}	-8.385575×10^{-2}	-1.000779×10^{-1}	-7.002453×10^{-2}	-7.547018×10^{-2}	-9.007010×10^{-2}	-6.302208×10^{-2}
1.0	7.221744×10^{-1}	8.618540×10^{-1}	6.065834×10^{-1}	7.264151×10^{-8}	3.331062×10^{-8}	3.204006×10^{-8}	7.264151×10^{-8}	3.331062×10^{-8}	3.204006×10^{-8}

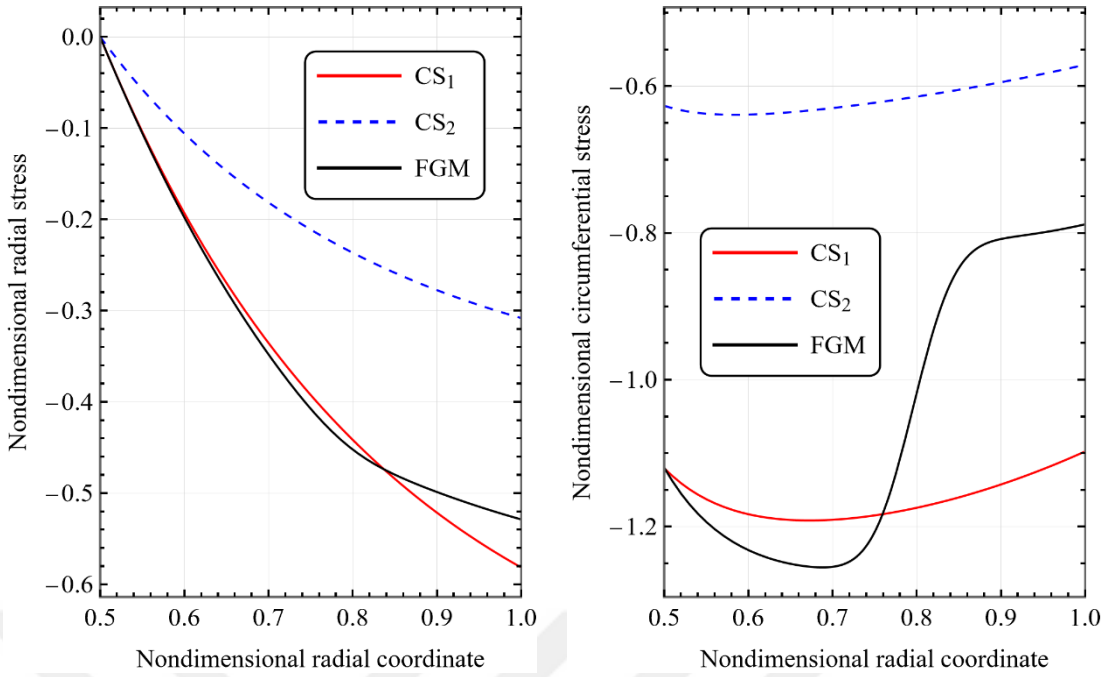

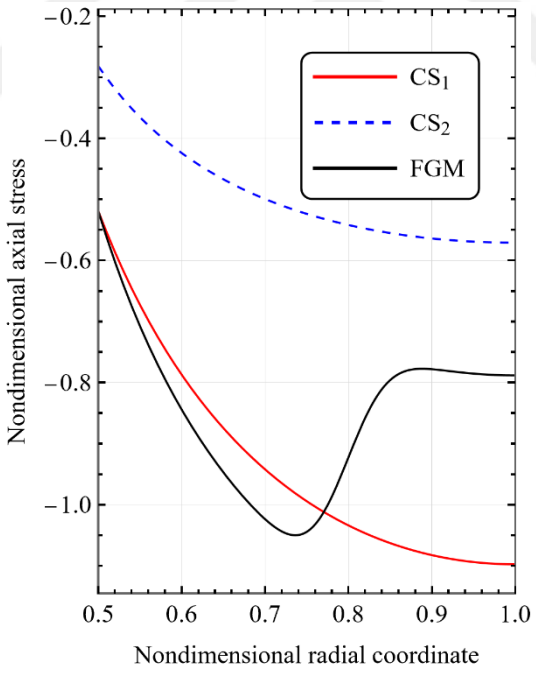

(c)

Figure 4.11: Variations of (a) the radial stress σ_r, (b) the circumferential stress σ_θ, and (c) the axial stress σ_z with r for the CS_1, CS_2, and FGM tubes subjected to their corresponding elastic limit heat loads considered in Sample Problem 2

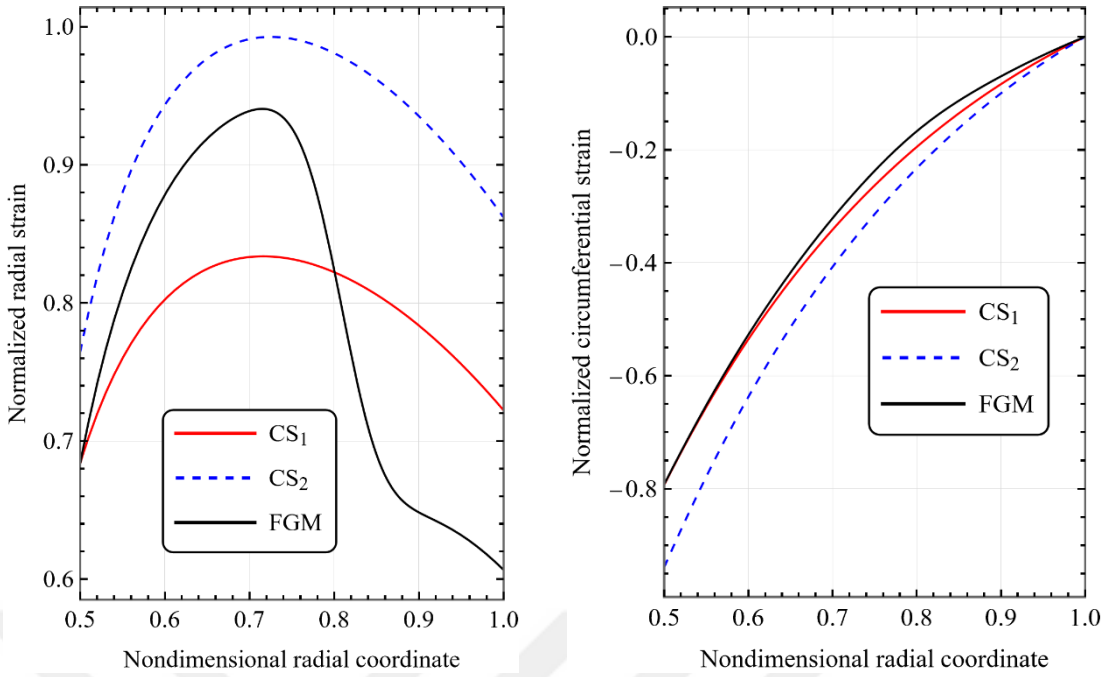

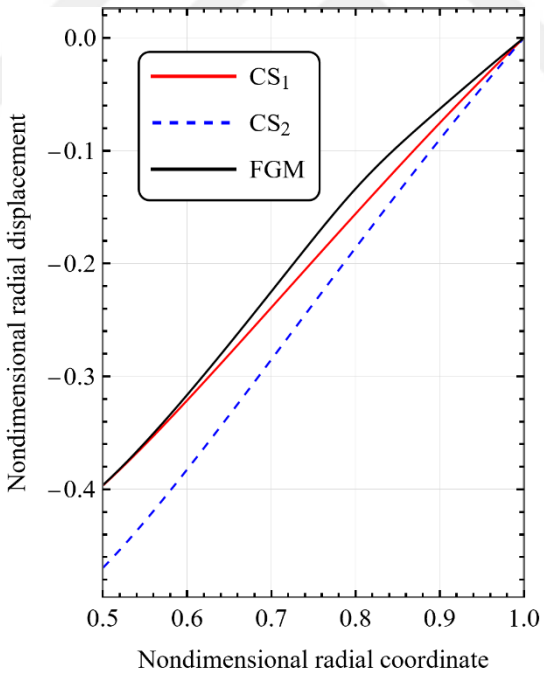

Figure 4.12: Variations of (a) the radial strain ε_r, (b) the circumferential strain ε_θ, and (c) the radial displacement u with r for the CS_1, CS_2, and FGM tubes subjected to their corresponding elastic limit heat loads considered in Sample Problem 2

CHAPTER 5

SUMMARY AND CONCLUSION

In this study, thermoelastic behavior of infinitely long FGM tubes with fixed ends that have temperature dependent material properties are investigated. The tubes are subjected to axisymmetric thermal and mechanical loadings. The formulations are derived under the assumptions of small deformations and a state of plane strain. The thermal and mechanical properties of the tubes are assumed to be graded along radial directions of the tubes.

The FGM material is considered to be formed from two constituents. These two constituents are Inconel 718 and Ti-6Al-4V. The effective material properties are determined by using the rule of mixtures. The formulation also accounts for the temperature dependency of the material properties. Since the material properties of each constituent forming the FGM are temperature-dependent, the properties of the FGM are also temperature-dependent. The variation of the constituents along the radial direction of the tube is described by a new form of function based on error function. With this proposed function it is possible to define a smooth and controlled grading of constituents at the desired locations within the range of radial coordinate.

Two sample problems are considered in the study. In each problem, for comparison, three different solutions are obtained. These are the solutions for the tubes made of a) constituent 1 (Inconel 718), (b) constituent 2 (Ti-6Al-4V), and (c) FGM. Thermal and mechanical problems are numerically solved using Mathematica.

First, the thermal problem is solved, and the distributions of thermal variables (temperature and temperature gradient) are determined along the radial direction of the tube. Secondly, with the use of the thermal variables determined in the first step, the mechanical problem is solved and therefrom the distributions of stresses, strains and radial displacements along the radial direction of the tube are evaluated.

Dimensional variables are used in the numerical solutions of thermal problems. Normalized and dimensionless variables are used in the solutions of mechanical problems The FGM material is assumed to be elastic, and thus, the solutions are valid within the elastic range.

In the first sample problem, an FGM tube subjected to internal pressure is analyzed. It is assumed the temperature is prescribed at its inner and outer surfaces. The results show that for the FGM tube the internal pressure that causes yielding is higher than those obtained for the homogeneous tubes made of constituent 1 or constituent 2. In the second sample problem, an FGM tube generating internal heat with a specified temperature at its inner surface, insulated outer surface, and embedded in a rigid casing is analyzed. As in the previous sample problem, the heat load required that causes yielding is higher than those for the homogeneous tubes made of constituent 1 or constituent 2. Moreover, in both problems, the mass per unit lengths of the FGM tubes at the elastic limit pressures and heat loads are lower than the tubes made of constituent 1. It is also observed that the stress, strain and radial displacement distributions of the FGM tubes are greatly affected by the material gradation.

These results obtained from the two sample problems show that, with proper material gradation (material tailoring) structural elements made of FGM may become more advantageous that those made of any of the constituents that form the FGM. The effects of gradation in the distributions of field variables within the tubes are clearly seen in those sample problems. How the material gradation affects these distributions is also dependent on the boundary conditions that are defined. For example, in the first sample problem where the temperature at the inner and outer surfaces is specified, the temperature distributions for all cases of the solutions do not differ that much.

REFERENCES

[1] V. Birman, & L. W. Byrd, “Modeling and analysis of functionally graded materials and structures.” *Applied Mechanics Reviews*, vol. 60, pp. 195–216, 2007.

[2] M. Koizumi, “FGM activities in Japan.” *Composites Part B*, vol. 28B, pp. 1–4, 1997.

[3] V. Boggarapu, R. Gujjala, S. Ojha, S. Acharya, P. Venkateswara babu, S. Chowdary, & D. Kumar Gara, “State of the art in functionally graded materials.” *Composite Structures*, vol. 262, pp. 1–29, 2021.

[4] B. Saleh, J. Jiang, R. Fathi, T. Al-hababi, Q. Xu, L. Wang, D. Song, & A. Ma, “30 years of functionally graded materials: An overview of manufacturing methods, applications and future challenges.” *Composites Part B: Engineering*, vol. 201, pp. 1–46, 2020.

[5] P. Shi, J. Xie, & X. Li, “Multilayer heterostructure inhomogeneous model for pressurized functionally graded annular structures (cylinder/sphere/annulus) with arbitrary elastic property along the radial direction.” *Composite Structures*, vol. 322, pp. 1–40, 2023.

[6] N. Noda, “Thermal stresses in materials with temperature-dependent properties.” *Applied Mechanics Reviews*, vol. 44, pp. 383-397, 1991.

[7] J. M. C. Duhamel, “Second mémoire sur les phénomènes thermomécaniques.” *Journal de l'École Polytechnique*, vol. 15, pp. 1-15, 1837.

[8] W. Voigt, *Lehrbuch der kristallphysik*. Leipzig&Berlin, 1910, pp 1-964.

[9] H. Jeffreys, “The thermodynamics of an elastic solid.” *Proceedings of the Cambridge Philosophical Society*, vol. 26, 1930.

[10] M. A. Biot, “Thermoelasticity and irreversible thermodynamics.” *Journal of Applied Physics*, vol. 27, pp. 240-253, 1956.

[11] S. R. De Groot, *Thermodynamics of irreversible processes*. Amsterdam: North-Holland Publishing Company, 1952.

[12] W. K. Nowacki, "Progress in thermoelasticity," in *Vlllth European Mechanics Colloquium*, 1967, pp. 1-61.

[13] E. Melan, & H. Parkus, *Wärmespannungen infolge stationärer Temperaturfelder*. Wien: Springer-Verlag, 1953.

[14] H. Parkus, *Instationäre wärmespannungen*. Wien: Springer-Verlag, 1959.

[15] B.A. Boley, & J. H. Weiner, *Theory of thermal stresses*. New York: McGraw-Hill Book Company, 1960.

[16] W. K. Nowacki, *Thermoelasticity*. Oxford: Pergamon Press, 1962.

[17] T. Suhara, "Elasticity of steel strained by unequal heating." *Journal of the Japan Society of Mechanical Engineers*, vol. 21, pp. 25-63, 1918.

[18] T. Koizumi, & T. Taniwaki, "Thermal stress in a solid circular cylinder exhibiting temperature-dependent properties." *Transactions of the Japan Society of Mechanical Engineers*, vol. 31, pp. 9-15, 1965.

[19] A. M. El'Karamani, "Stress concentration in a medium with temperature-dependent properties." *Prikladnaya Mekhanika*, vol. 14, pp. 284-290, 1978.

[20] P. Stanley, & F. S. Chau, "The effects of the temperature-dependence of properties on the thermal stresses in cylinders" in *Thermal Stresses in Severe Environments,* New York: Plenum, 1980, pp. 61-80.

[21] N. Noda, & Y. Daichyo, "Transient thermoelastic problem in a long circular cylinder with temperature dependent properties." *Transactions of the Japan Society of Mechanical Engineers Series A*, vol. 53, pp. 559-565, 1987.

[22] N. Noda "Thermal stresses in materials with temperature-dependent properties" in *Thermal Stress,* North-Holland&Amsterdam, pp. 391-483, 1986.

[23] Y.S. Touloukian, “Vol. 1: Conductivity—Metallic elements and alloys” in *Thermophysical properties of matter,* New York: IFI/Plenum, 1970.

[23] Y.S. Touloukian, “Vol. 12: Thermal expansion—Metallic elements and alloys” in *Thermophysical properties of matter,* New York: IFI/Plenum, 1975.

[25] Y. Orcan, & M. Gulgec, “Influence of the temperature dependence of the yield stress on the stress distribution in a heat-generating tube with free ends.” *Journal of Thermal Stresses*, vol. 23, pp. 529–547, 2000.

[26] Y. Orcan, & A. N. Eraslan, “Thermal stresses in elastic-plastic tubes with temperature-dependent mechanical and thermal properties.” *Journal of Thermal Stresses*, vol. 24, pp. 1097–1113, 2001.

[27] A. N. Eraslan, & H. Argeso, “Computer solutions of plane strain axisymmetric thermomechanical problems.” *Turkish Journal of Engineering and Environmental Sciences*, vol. 29, pp. 369–381, 2005.

[28] H. Argeso, & A. N. Eraslan, “On the use of temperature-dependent physical properties in thermomechanical calculations for solid and hollow cylinders.” *International Journal of Thermal Sciences*, vol. 47, pp. 136–146, 2008.

[29] A. M. Zenkour, & I. A. Abbas, “A generalized thermoelasticity problem of an annular cylinder with temperature-dependent density and material properties.” *International Journal of Mechanical Sciences*, vol. 84, pp. 54–60, 2014.

[30] I. A. Abbas, “Generalized thermoelastic interactions in a hollow cylinder with temperature-dependent material properties.” *Journal of Thermal Science and Technology*, vol. 12, pp. 1–9, 2017.

[31] M. B. Bever, & P. E. Duwez, “Gradients in composite materials.” *Materials Science and Engineering*, vol. 10, pp. 1-8, 1972.

[32] M. Shen, & M. B. Bever, “Gradients in polymeric materials.” *Journal of Materials Science*, vol. 7, pp. 741–746, 1972.

[33] Y. Miyamoto, W. A. Kaysser, B. H. Rabin, A. Kawasaki, and R. G. Ford, *Functionally graded materials: Design, processing and applications*. Kluwer Academic Publishers, 1999, pp. 1-330.

[34] V. Bhavar, P. Kattire, S. Thakare, S. Patil, and R. K. P. Singh, “A review on functionally gradient materials (FGMs) and their applications,” *IOP Conference Series: Materials Science and Engineering*, vol. 226, pp. 1-9, 2017.

[35] S. Aysha CPM, B. Varghese, & A. Baby, “A review on functionally graded materials.” *The International Journal of Engineering and Science (IJES)*, vol. 3, pp. 90–101, 2014.

[36] M. Koizumi, & M. Niino, “Overview of FGM research in Japan.” *MRS Bulletin*, vol. 1, pp. 19–21, 1995.

[37] P. K. Chauhan, & Dr. S. Khan, “Functionally graded materials - A review on application of finite element method.” *International Journal of Advances in Production and Mechanical Engineering*, vol. 2, pp. 1–6, 2016.

[38] I. M. El-Galy, B. I. Saleh, & M. H. Ahmed, “Functionally graded materials classifications and development trends from industrial point of view.” *SN Applied Sciences*, 2019.

[39] Shen, H. *Functionally graded materials nonlinear analysis of plates and shells*. New York: CRC Press, 2009, pp. 1-266.

[40] I. Elishakoff., D. Pentaras, & C. Gentilini, *Mechanics of functionally graded material structures*. Singapore: World Scientific Publishing Co. Pte. Ltd., 2016, pp. 1-323.

[41] J. Ying, C. F. Lü, & W. Q. Chen, “Two-dimensional elasticity solutions for functionally graded beams resting on elastic foundations.” *Composite Structures*, vol. 84, pp. 209–219, 2008.

[42] X. L. Peng, & X. F. Li, “Thermal stress in rotating functionally graded hollow cylinders.” *Journal of Thermal Stress*, vol. 21, pp. 39–53, 1998.

[43] G. J. Nie, Z. Zhong, & S. Chen, “Analytical solution for a functionally graded beam with arbitrary graded material properties.” *Composites Part B*, vol. 44, pp. 274–282, 2013.

[44] B. V. Sankar, & J. T. Tzeng, “Thermal stresses in functionally graded beams.” *AIAA Journal*, vol. 40, pp. 1228–1232, 2002.

[45] S. S. Vel, & R. C. Batra, “Exact solution for thermoelastic deformations of functionally graded thick rectangular plates.” *AIAA Journal*, vol. 40, pp. 1421–1433, 2002.

[46] S. S. Vel, & R. C. Batra, “Three-dimensional analysis of transient thermal stresses in functionally graded plates.” *International Journal of Solids and Structures*, vol. 40, pp. 7181–7196, 2003.

[47] Y. Ootao, & Y. Tanigawa, “Transient thermoelastic analysis for a multilayered hollow circular disk with piecewise power law nonhomogeneity.” *Journal of Thermal Stresses*, vol. 35, pp. 75–90, 2012.

[48] Y. Ootao, & M. Ishihara, “Three-dimensional solution for transient thermoelastic problem of a functionally graded rectangular plate with piecewise exponential law.” *Composite Structures*, vol. 106, pp. 672–680, 2013.

[49] M. Nemat-Alla, K. I. E. Ahmed, & I. Hassab-Allah, “Elastic-plastic analysis of two-dimensional functionally graded materials under thermal loading.” *International Journal of Solids and Structures*, vol. 46, pp. 2774–2786, 2009.

[50] J. N. Reddy, & C. D. Chin, “Thermomechanical analysis of functionally graded cylinders and plates.” *Journal of Thermal Stresses*, vol. 21, pp. 593–626, 1998.

[51] G. N. Praveen, C. D. Chin, & J. N. Reddy, “Thermoelastic analysis of functionally graded ceramic-metal cylinder.” *Journal of Engineering Mechanics*, vol. 125, pp. 1259–1267, 1999.

[52] B. L. Wang, & Y. W. Mai, “Transient one-dimensional heat conduction problems solved by finite element.” *International Journal of Mechanical Sciences*, vol. 47, pp. 303–317, 2005.

[53] H. K. Ching, & J. K. Chen, “Thermal stress analysis of functionally graded composites with temperature-dependent material properties.” *Journal of Mechanics of Materials and Structures*, vol. 2, pp. 633–653, 2007.

[54] T. Darabseh, N. Yilmaz, & M. Bataineh, “Transient thermoelasticity analysis of functionally graded thick hollow cylinder based on Green-Lindsay model.” *International Journal of Mechanics and Materials in Design*, vol. 8, pp. 247–255, 2012.

[55] K. M. Liew, S. Kitipornchai, X. Z. Zhang, & C. W. Lim, “Analysis of the thermal stress behaviour of functionally graded hollow circular cylinders.” *International Journal of Solids and Structures*, vol. 40, pp. 2355–2380, 2003.

[56] R. W. Zimmerman, & M. P. Lutz, “Thermal stresses and thermal expansion in a uniformly heated functionally graded cylinder.” *Journal of Thermal Stresses*, vol. 22, pp. 177–188, 1999.

[57] J.-Q. Tarn, “Exact solutions for functionally graded anisotropic cylinders subjected to thermal and mechanical loads.” *International Journal of Solids and Structures*, vol. 38, pp. 8189–8206, 2001.

[58] Z. S. Shao, T. J. Wang, & K. K. Ang, “Transient thermo-mechanical analysis of functionally graded hollow circular cylinders.” *Journal of Thermal Stresses*, vol. 30, pp. 81–104, 2007.

[59] M. Z. Nejad, & G. H. Rahimi, “Deformations and stresses in rotating FGM pressurized thick hollow cylinder under thermal load.” *Scientific Research and Essay*, vol. 4, pp. 131–140, 2009.

[60] X. L. Peng, & X. F. Li, “Transient response of temperature and thermal stresses in a functionally graded hollow cylinder.” *Journal of Thermal Stresses*, vol. 33, pp. 485–500, 2010.

[61] M. Jabbari, S. Sohrabpour, & M. R. Eslami, “Mechanical and thermal stresses in a functionally graded hollow cylinder due to radially symmetric loads.” *International Journal of Pressure Vessels and Piping*, vol. 79, pp. 493–497, 2002.

[62] T. Akis, “Elastoplastic analysis of functionally graded spherical pressure vessels.” *Computational Materials Science*, vol. 46, pp. 545–554, 2009.

[63] T. Akış, “Isı etkisi altındaki fonksiyonel derecelendirilmiş malzemeden yapılmış uzun tüplerde plastik akmanın başlaması.” *J. Fac. Eng. Arch. Gazi Univ.*, vol. 21, pp. 737–743, 2006.

[64] A. N. Eraslan, & T. Akis, “Analytical solutions to elastic functionally graded cylindrical and spherical pressure vessels.” *Journal of Multidisciplinary Engineering Science and Technology (JMEST)*, vol. 2, pp. 3159–3199, 2015.

[65] D. Sharma, & R. Kaur, “Thermoelastic analysis of FGM hollow cylinder for variable parameters and temperature distributions using FEM.” *Nonlinear Engineering*, vol. 9, pp. 256–264, 2020.

[66] B. L. Wang, & Z. H. Tian, “Application of finite element-finite difference method to the determination of transient temperature field in functionally graded materials.” *Finite Elements in Analysis and Design*, vol. 41, pp. 335–349, 2005.

[67] R. Hill, “A self-consistent mechanics of composite materials.” *Journal of the Mechanics and Physics of Solids*, vol. 13, pp. 213–222, 1965.

[68] T. Mori, & K. Tanaka, “Average stress in matrix and average elastic energy of materials with misfitting inclusions.” *Acta Metallurgica*, vol. 21, pp. 571–574, 1973.

[69] Y. Benveniste, “A new approach to the application of Mori-Tanaka’s theory in composite materials.” *Mechanics of Materials*, vol. 6, pp. 147–157, 1987.

[70] L. J. Gibson, M. F. Ashby, G. N. Karam, U. Wegst, & H. R. Shercliff, “Mechanical properties of natural materials. II. Microstructures for mechanical efficiency.” *Proceedings of the Royal Society of London Series A*, vol. 450, pp. 141–162, 1995.

[71] Wolfram Research, Inc. (2024). *Mathematica* (Version 14.1).

[72] N. Noda, R. B. Hetnarski, and Y. Tanigawa, *Thermal Stresses (2nd ed.)*. Londra: Taylor & Francis, 2003

[73] Weisstein, E. W. "Erf." from MathWorld--A Wolfram Web Resource. [Online]. Available: https://mathworld.wolfram.com/Erf.html [2024].

[74] V. A. Popovich, E. V. Borisov, V. Heurtebise, T. Riemslag, A. A. Popovich, & V. S. Sufiiarov, “Creep and thermomechanical fatigue of functionally graded Inconel 718 produced by additive manufacturing.” *TMS 2018 147th Annual Meeting & Exhibition Supplemental Proceedings*, pp. 85–97, 2018.

[75] X. Zhang, L. Li, & F. Liou, “Additive manufacturing of stainless steel – copper functionally graded materials via Inconel 718 interlayer.” *Journal of Materials Research and Technology*, vol. 15, pp. 2045–2058, 2021.

[76] S. W. Yang, J. Yoon, H. Lee, & D. S. Shim, “Defect of functionally graded material of Inconel 718 and STS 316L fabricated by directed energy deposition and its effect on mechanical properties.” *Journal of Materials Research and Technology*, vol. 17, pp. 478–497, 2022.

[77] S. H. Kim, H. Lee, S. M. Yeon, C. Aranas, K. Choi, J. Yoon, S. W. Yang, & H. Lee, “Selective compositional range exclusion via directed energy deposition to produce a defect-free Inconel 718/SS 316L functionally graded material.” *Additive Manufacturing*, vol. 47, pp. 1–13, 2021.

[78] Y. Geng, Microstructural functionally graded Ti-6Al-4V via advanced laser-based technologies. NUI Galway, 2021.

[79] Y. Geng, B. Phelan, R. Raghavendra, & N. Harrison, “Single-step process of microstructural functionally graded Ti6Al4V by laser powder bed fusion additive manufacturing.” *Welding in the World*, vol. 64, pp. 1357–1366, 2020.

[80] C. W. Park, R. N. Hajra, S. H. Kim, S. H. Lee, & J. H. Kim, “Optimizing multi-interlayered additive manufacturing for high strength robust joints in Inconel 718 and Ti–6Al–4V alloys.” *Journal of Materials Research and Technology*, vol. 25, pp. 855–872, 2023.

[81] S. Ji, Z. Sun, W. Zhang, X. Chen, G. Xie, & H. Chang, “Microstructural evolution and high temperature resistance of functionally graded material Ti-6Al-4V/Inconel 718 coated by directed energy deposition-laser.” *Journal of Alloys and Compounds*, vol. 848, pp. 1–16, 2020.

[82] X. L. Gao, J. Liu, & L. J. Zhang, “Dissimilar metal welding of Ti6Al4V and Inconel 718 through pulsed laser welding-induced eutectic reaction technology.” *International Journal of Advanced Manufacturing Technology*, vol. 96, pp. 1061–1071, 2018.

[83] J. Liu, H. Liu, X. L. Gao, & H. Yu, “Microstructure and mechanical properties of laser welding of Ti6Al4V to Inconel 718 using Nb/Cu interlayer.” *Journal of Materials Processing Technology*, vol. 277, pp. 1–13, 2020.

[84] B. Onuike, & A. Bandyopadhyay, “Additive manufacturing of Inconel 718 – Ti6Al4V bimetallic structures.” *Additive Manufacturing*, vol. 22, pp. 844–851, 2018.

[85] *Material Property Database: MPDB Software*, JAHM Software, Inc., 29 Valley Rd., North Reading, MA, 01864-1740 (http://www.jahm.com).

[86] Mendelson, *A. Plasticity: Theory and Application*. New York: Macmillan, 1968.